

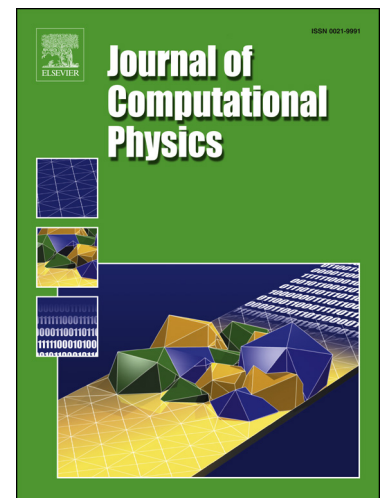
# Journal Pre-proof

Very high order WENO schemes using efficient smoothness indicators

Conghai Wu, Ling Wu, Hu Li and Shuhai Zhang

PII: S0021-9991(21)00050-4  
DOI: <https://doi.org/10.1016/j.jcp.2021.110158>  
Reference: YJCPH 110158

To appear in: *Journal of Computational Physics*



Please cite this article as: C. Wu, L. Wu, H. Li et al., Very high order WENO schemes using efficient smoothness indicators, *Journal of Computational Physics*, 110158, doi: <https://doi.org/10.1016/j.jcp.2021.110158>.

This is a PDF file of an article that has undergone enhancements after acceptance, such as the addition of a cover page and metadata, and formatting for readability, but it is not yet the definitive version of record. This version will undergo additional copyediting, typesetting and review before it is published in its final form, but we are providing this version to give early visibility of the article. Please note that, during the production process, errors may be discovered which could affect the content, and all legal disclaimers that apply to the journal pertain.

© 2021 Published by Elsevier.

**Highlights**

- Very high order WENO schemes using efficient smoothness indicators were proposed.
- They can do well both in smooth and discontinuous region with high time efficiency.
- They will reduce to the underlying linear schemes for monochromatic waves.
- A predetermined order reduction method is proposed for Euler equations.

# Very high order WENO schemes using efficient smoothness indicators

Conghai Wu <sup>1</sup>, Ling Wu <sup>2</sup>, Hu Li <sup>1</sup>, Shuhai Zhang <sup>1</sup>

January 27, 2021

1.State Key Laboratory of Aerodynamics, China Aerodynamics Research and Development Center, Mianyang, Sichuan 621000, China,

2.School of Computer Science and Technology, Southwest University of Science and Technology, Mianyang, Sichuan 621000, China

## Abstract

Very high order weighted essentially non-oscillatory (WENO) schemes can obtain more accurate results than those relatively low order WENO schemes for many problems. However, as the order increases, the candidate sub-stencils of WENO schemes will contain more node points. Then, the classical smoothness indicators become very complex and need much more floating point operations. Although they could be written in a more succinct form which is a sum of perfect squares, only a little improvement of the computational efficiency is obtained. Furthermore, for the power parameter  $p$  in the nonlinear weights of the previous  $(2r-1)$ th order WENO schemes, only the range of choices is given and the optimal value could be problem dependent. In this article, another class of very high order WENO schemes is constructed by using more efficient smoothness indicators. Compared with very high order WENO schemes using classical smoothness indicators, the new ones are more time efficient, and less error prone for programming. Furthermore, they have the same approximate dispersion relation (ADR) as their underlying linear schemes. And a more important advantage is that they have both good behavior near critical points and good stability near discontinuities. For Euler equations, a predetermined order reduction technique including two inequalities is proposed to deal with the problems caused by interactions between discontinuities of different characteristic fields. One inequality is constructed using this kind of smoothness indicators of pressure to suppress the non-physical oscillations. And the other is proposed according to the governing equation of the pressure to prevent the emergence of negative pressure. Several test problems are presented to demonstrate the good properties of the proposed WENO schemes.

**Keywords:** WENO scheme, smoothness indicator, high order scheme, finite difference scheme

## 1 Introduction

Hyperbolic conservation laws are often used to mathematically describe the flow of gas dynamics, shallow water and magneto-hydro-dynamics (MHD). The most significant feature of hyperbolic conservation laws is that discontinuities can appear even for smooth initial data. This makes it difficult to numerically simulate these problems. For resolving the discontinuities and other structures in the flow, many techniques have been developed[1, 2, 3].

Weighted essentially non-oscillatory (WENO) scheme is one of the solution which has been quite successful in applications of these fields[4]. The WENO scheme appeared firstly at the work of Liu et al.[5], which is a convex combination of the approximations on some candidate stencils. This kind of WENO schemes employs the finite volume framework and obtains one extra accuracy order in the procedure of combination. However, the optimal accuracy order on the whole stencil could not be recovered if the underlying scheme has an accuracy order higher than 3. To solve this problem, Jiang and Shu proposed an improved smoothness indicator[6], with which the corresponding  $(2r-1)$ -point WENO scheme can obtain the optimal  $(2r - 1)$ th order of accuracy. The WENO schemes in that work were proposed in the finite difference framework. Then,  $(2r - 1)$ th order WENO schemes were investigated for large  $r$ [7, 8], in which a  $(2r-1)$ -point stencil is adopted and divided into  $r$  candidate sub-stencils with  $r$ -point. In this study, we will focus on finite difference WENO schemes in this framework.

However, WENO schemes above with relatively low accuracy order cannot obtain very good results for those problems containing small scale structures. To capture discontinuities and other structures of the flow more accurately, many methods have been developed based on the methodology of WENO schemes. The mapped WENO schemes proposed by Henrick et al. is one of them, although the initial purpose of the mapping procedure

is to overcome the problem that the previous five-point WENO scheme cannot achieve fifth order accuracy near some critical points [9]. Then, Borges et al. modified the way of computing the nonlinear weights, and the resultant scheme called as Z-type WENO scheme can obtain similar results as the mapped WENO scheme but with higher time efficiency [10]. The Z-type WENO scheme was extended to higher order cases and was further improved in [11, 12]. With modified smoothness indicators and the technique of Z-type WENO scheme, some improved WENO schemes were proposed [13, 14]. In [15], a WENO scheme using both the mapped procedure and the technique of Z-type WENO scheme was proposed. Some high order finite difference shock capturing schemes employ frameworks different from the (2r-1)-point WENO scheme mentioned above. The six-point WENO schemes proposed in [16, 17] use an additional downwind sub-stencil to reduce the numerical dissipation. Besides that, a five-point WENO scheme proposed by Zhu and Qiu [18] employs the whole five-point stencil and two two-point stencils as the candidate stencils. Qiu and Shu [19] proposed the Hermite WENO schemes which could use narrower stencil to achieve high order accuracy. In Hermite WENO scheme, both the function and its first derivative are evolved in time, which makes them more complex and time-consuming. Hybridization of WENO scheme with other low dissipative schemes is another kind of solutions, for which the WENO scheme is used for capturing discontinuities. In [20], a sixth order central finite difference scheme is combined with a fifth order WENO scheme. Pirozzoli [21] proposed a conservative hybrid compact-WENO scheme in a component-wise fashion, which was then improved to a characteristic-wise type by Ren et al. [22]. The hybrid compact-WENO scheme was further improved by using a lower dissipative compact scheme [23] and a specific technique of hybridization proposed for Euler equations [24]. Compact difference schemes based on the values of half node points obtained from WENO interpolation were proposed in [25, 26]. The optimized WENO scheme is also a kind of choices, whose linear weights are optimized to obtain a better spectral property [27, 16]. However, the optimization will lead to a reduction of the accuracy order. It is better to obtain good spectral property without sacrificing accuracy order. An example is the FWENO7 scheme, which however is not a very good choice for resolving discontinuities [14].

Very high order WENO schemes can obtain more accurate results than those relatively low order ones for many problems. The numerical viscosities of high order WENO schemes and the resolution power of them were investigated in [28], and a conclusion was drawn that high order WENO schemes are more time efficient to reach the same resolution. The numerical behaviors of the classical very high order WENO schemes could be found in [7, 8]. Targeted ENO (TEN0) schemes are also very high order accurate but with better stability property [29]. In high order TEN0 schemes, the candidate stencils include three three-point ones and some others with gradually increased width, and they will be abandoned if containing strong discontinuities. However, there are some free parameters in these schemes which need fine tuning for different problems. The adaptive order WENO schemes in [30] are obtained by nonlinear hybridization of a higher order centered stencil and a stable  $r = 3$  CWENO scheme, and seem to capture discontinuities very crisply without needing any steepening step. These high order WENO schemes adopt the classical smoothness indicators which were proposed in [6]. However, it could be found that this kind of smoothness indicators has many items for  $r \geq 4$ , and becomes much more complex with increasing of  $r$ . Particularly the coefficients table for  $r = 9$  even occupies two pages [8]. Although each of them could be written as a sum of perfect squares [31, 32], the computational cost is still very high. The fast WENO schemes [32] employ a class of succinct smoothness indicators, but very high order fast WENO schemes will encounter serious problems which will be shown in the present work.

In this paper, a class of very high order WENO schemes which employs efficient smoothness indicators will be presented. It can be considered as a generalization of the WENO7-S scheme [14]. This paper is organized as follows: in section 2, the new WENO schemes are constructed. In section 3, the time integration methods and the boundary treatment are introduced. The accuracy order and the time efficiency are considered in section 4 and 5 respectively. Then, numerical tests for 1D scalar problem are carried out in section 6. The numerical simulations for Euler equations are presented in section 7. In the last section, the conclusions are drawn.

## 2 Construction of the new WENO schemes

Consider the scalar hyperbolic conservation law given by

$$\frac{\partial u}{\partial t} + \frac{\partial f}{\partial x} = 0, \quad (1)$$

where  $u(x, t)$  is a conserved quantity,  $f(u(x, t))$  is the flux. For a uniform grid  $x_i = x_L + (i - 0.5) \cdot h$ ,  $h = (x_R - x_L)/N$ ,  $i = 1, \dots, N$ , where  $x_L$  and  $x_R$  are the positions of the left and the right boundaries respectively, the half node point is given as  $x_{i \pm 1/2} = x_i \pm h/2$ . The semi-discretized conservative difference scheme for Eq.(1) can be written as

$$\frac{du_i(t)}{dt} = -\frac{1}{h}(\hat{f}_{i+1/2} - \hat{f}_{i-1/2}), \quad (2)$$

where numerical fluxes  $\hat{f}_{i \pm 1/2}$  can be obtained from node values of  $f(u(x, t))$ . As the numerical flux is obtained, the solution can be advanced by time methods such as strong stability preserving (SSP) Runge-Kutta type

methods[33].

## 2.1 The classical (2r-1)-point WENO scheme

In (2r-1)-point WENO scheme, the numerical flux  $\hat{f}_{i+1/2}$  is obtained from the stencil  $S = \{x_{i-r+1}, x_{i-r+2}, \dots, x_{i+r-1}\}$  with an upwind bias, and the  $r$  candidate sub-stencils are given as  $S_k = \{x_{i-r+k+1}, x_{i-r+k+2}, \dots, x_{i+k}\}$ ,  $k = 0, 1, \dots, r-1$ . This is under the assumption that  $\partial f / \partial u > 0$ . As  $\partial f / \partial u < 0$ , both the stencil and the flux can be obtained by symmetry. If the sign of  $\partial f / \partial u$  could not be determined, a flux splitting method such as Lax-Friedrichs splitting should be employed[6].

The numerical fluxes obtained from the candidate stencils are

$$\hat{f}_{i+1/2}^{r,k} = \sum_{l=0}^{r-1} c_{l,k}^r f_{i-r+k+l+1}, \quad k = 0, 1, \dots, r-1. \quad (3)$$

The coefficients  $c_{l,k}^r$  for  $r \leq 9$  are given in Table 1. And a method to obtain the expression of numerical flux is given in the appendix.

The numerical flux of the (2r-1)-point high order WENO scheme is a convex combination of these fluxes.

$$\hat{f}_{i+1/2}^r = \sum_{k=0}^{r-1} \omega_k^r \hat{f}_{i+1/2}^{r,k}. \quad (4)$$

For classical WENO schemes, the weights  $\omega_k^r$  are defined as

$$\omega_k^{r(JS)} = \frac{\alpha_k^r}{\sum_{l=0}^{r-1} \alpha_l^r}, \quad \alpha_k^r = \frac{d_k^r}{\left(\beta_k^{r(JS)}\right)^p + \varepsilon}, \quad k = 0, 1, \dots, r-1. \quad (5)$$

Power parameter  $p$  is suggested as an integer belong to  $[2, r]$ [8].  $\varepsilon$  is a tiny positive value bounding the denominator, whose effect on the accuracy order has been analyzed in [34].  $d_k^r$  are the optimal weights which could be obtained by using Taylor expansion. In Table 2,  $d_k^r$  are given for  $r \leq 9$ . If  $d_k^r$  are assigned to  $\omega_k^r$  for  $k = 0, 1, \dots, r-1$ , WENO scheme (4) will become the (2r-1)th order upstream central linear scheme.

$$\hat{f}_{i+1/2}^{r(L)} = \sum_{l=-r+1}^{r-1} a_l^r f_{i+l}. \quad (6)$$

Coefficients  $a_l^r$  for  $r \leq 9$  are tabulated in Table 3.

$\beta_k^{r(JS)}$  are the smoothness indicators given as[6]

$$\beta_k^{r(JS)} = \sum_{l=1}^{r-1} h^{2l-1} \int_{x_{i-1/2}}^{x_{i+1/2}} \left( \frac{d^l}{dx^l} \hat{f}_k(x) \right)^2 dx, \quad k = 0, 1, \dots, r-1, \quad (7)$$

where  $\hat{f}_k(x)$  are the reconstruction polynomials of fluxes on sub-stencils  $S_k$ . The explicit expressions of  $\beta_k^{r(JS)}$  for  $r = 2$  are

$$\begin{aligned} \beta_0^{2(JS)} &= (f_i - f_{i-1})^2, \\ \beta_1^{2(JS)} &= (-f_i + f_{i+1})^2, \end{aligned} \quad (8)$$

And  $\beta_k^{r(JS)}$  for  $r = 3$  are

$$\begin{aligned} \beta_0^{3(JS)} &= \frac{1}{4}(f_{i-2} - 4f_{i-1} + 3f_i)^2 + \frac{13}{12}(f_{i-2} - 2f_{i-1} + f_i)^2, \\ \beta_1^{3(JS)} &= \frac{1}{4}(f_{i+1} - f_{i-1})^2 + \frac{13}{12}(f_{i-1} - 2f_i + f_{i+1})^2, \\ \beta_2^{3(JS)} &= \frac{1}{4}(3f_i - 4f_{i+1} + f_{i+2})^2 + \frac{13}{12}(f_i - 2f_{i+1} + f_{i+2})^2. \end{aligned} \quad (9)$$

Table 1: Coefficients  $c_{l,k}^r$  in the fluxes on the  $r$  sub-stencils of  $(2r - 1)$ -point WENO schemes for  $r \leq 9$ .

$r$	$l$	k=0	k=1	k=2	k=3	k=4	k=5	k=6	k=7	k=8
1	0	1								
2	0	$\frac{-1}{2}$	$\frac{3}{2}$							
	1	$\frac{1}{2}$	$\frac{1}{2}$							
3	0	$\frac{2}{6}$	$\frac{-7}{6}$	$\frac{11}{6}$						
	1	$\frac{-1}{6}$	$\frac{5}{6}$	$\frac{2}{6}$						
	2	$\frac{2}{6}$	$\frac{5}{6}$	$\frac{-1}{6}$						
4	0	$\frac{-3}{12}$	$\frac{13}{12}$	$\frac{-23}{12}$	$\frac{25}{12}$					
	1	$\frac{1}{12}$	$\frac{-5}{12}$	$\frac{13}{12}$	$\frac{3}{12}$					
	2	$\frac{-1}{12}$	$\frac{7}{12}$	$\frac{7}{12}$	$\frac{-1}{12}$					
	3	$\frac{3}{12}$	$\frac{13}{12}$	$\frac{-5}{12}$	$\frac{1}{12}$					
5	0	$\frac{12}{60}$	$\frac{-63}{60}$	$\frac{137}{60}$	$\frac{-163}{60}$	$\frac{137}{60}$				
	1	$\frac{-3}{60}$	$\frac{17}{60}$	$\frac{-43}{60}$	$\frac{77}{60}$	$\frac{12}{60}$				
	2	$\frac{2}{60}$	$\frac{-13}{60}$	$\frac{47}{60}$	$\frac{27}{60}$	$\frac{-3}{60}$				
	3	$\frac{-3}{60}$	$\frac{27}{60}$	$\frac{47}{60}$	$\frac{-13}{60}$	$\frac{2}{60}$				
	4	$\frac{12}{60}$	$\frac{77}{60}$	$\frac{-43}{60}$	$\frac{17}{60}$	$\frac{-3}{60}$				
6	0	$\frac{-10}{60}$	$\frac{62}{60}$	$\frac{-163}{60}$	$\frac{237}{60}$	$\frac{-213}{60}$	$\frac{147}{60}$			
	1	$\frac{2}{60}$	$\frac{-13}{60}$	$\frac{37}{60}$	$\frac{-63}{60}$	$\frac{87}{60}$	$\frac{10}{60}$			
	2	$\frac{-1}{60}$	$\frac{7}{60}$	$\frac{-23}{60}$	$\frac{57}{60}$	$\frac{22}{60}$	$\frac{-2}{60}$			
	3	$\frac{1}{60}$	$\frac{-8}{60}$	$\frac{37}{60}$	$\frac{37}{60}$	$\frac{-8}{60}$	$\frac{1}{60}$			
	4	$\frac{-2}{60}$	$\frac{22}{60}$	$\frac{57}{60}$	$\frac{-23}{60}$	$\frac{7}{60}$	$\frac{-1}{60}$			
	5	$\frac{10}{60}$	$\frac{87}{60}$	$\frac{-63}{60}$	$\frac{37}{60}$	$\frac{-13}{60}$	$\frac{2}{60}$			
7	0	$\frac{60}{420}$	$\frac{-430}{420}$	$\frac{1334}{420}$	$\frac{-2341}{420}$	$\frac{2559}{420}$	$\frac{-1851}{420}$	$\frac{1089}{420}$		
	1	$\frac{-10}{420}$	$\frac{74}{420}$	$\frac{-241}{420}$	$\frac{4591}{420}$	$\frac{-591}{420}$	$\frac{669}{420}$	$\frac{60}{420}$		
	2	$\frac{4}{420}$	$\frac{-31}{420}$	$\frac{109}{420}$	$\frac{-241}{420}$	$\frac{459}{420}$	$\frac{130}{420}$	$\frac{-10}{420}$		
	3	$\frac{-3}{420}$	$\frac{25}{420}$	$\frac{-101}{420}$	$\frac{319}{420}$	$\frac{214}{420}$	$\frac{-38}{420}$	$\frac{4}{420}$		
	4	$\frac{4}{420}$	$\frac{-38}{420}$	$\frac{214}{420}$	$\frac{319}{420}$	$\frac{-101}{420}$	$\frac{25}{420}$	$\frac{-3}{420}$		
	5	$\frac{-10}{420}$	$\frac{130}{420}$	$\frac{459}{420}$	$\frac{-241}{420}$	$\frac{109}{420}$	$\frac{-31}{420}$	$\frac{4}{420}$		
	6	$\frac{60}{420}$	$\frac{669}{420}$	$\frac{-591}{420}$	$\frac{4591}{420}$	$\frac{-241}{420}$	$\frac{74}{420}$	$\frac{-10}{420}$		
8	0	$\frac{-105}{840}$	$\frac{855}{840}$	$\frac{-3065}{840}$	$\frac{6343}{840}$	$\frac{-8357}{840}$	$\frac{7323}{840}$	$\frac{-4437}{840}$	$\frac{2283}{840}$	
	1	$\frac{15}{840}$	$\frac{-125}{840}$	$\frac{463}{840}$	$\frac{-1007}{840}$	$\frac{1443}{840}$	$\frac{-1497}{840}$	$\frac{1443}{840}$	$\frac{105}{840}$	
	2	$\frac{-5}{840}$	$\frac{43}{840}$	$\frac{-167}{840}$	$\frac{393}{840}$	$\frac{-657}{840}$	$\frac{1023}{840}$	$\frac{225}{840}$	$\frac{-15}{840}$	
	3	$\frac{3}{840}$	$\frac{-27}{840}$	$\frac{113}{840}$	$\frac{-307}{840}$	$\frac{743}{840}$	$\frac{365}{840}$	$\frac{-55}{840}$	$\frac{5}{840}$	
	4	$\frac{-3}{840}$	$\frac{29}{840}$	$\frac{-139}{840}$	$\frac{533}{840}$	$\frac{533}{840}$	$\frac{-139}{840}$	$\frac{29}{840}$	$\frac{-3}{840}$	
	5	$\frac{5}{840}$	$\frac{-55}{840}$	$\frac{365}{840}$	$\frac{743}{840}$	$\frac{-307}{840}$	$\frac{113}{840}$	$\frac{-27}{840}$	$\frac{3}{840}$	
	6	$\frac{-15}{840}$	$\frac{225}{840}$	$\frac{1023}{840}$	$\frac{-657}{840}$	$\frac{393}{840}$	$\frac{-167}{840}$	$\frac{43}{840}$	$\frac{-5}{840}$	
	7	$\frac{105}{840}$	$\frac{1443}{840}$	$\frac{-1497}{840}$	$\frac{1443}{840}$	$\frac{-1007}{840}$	$\frac{463}{840}$	$\frac{-125}{840}$	$\frac{15}{840}$	
9	0	$\frac{280}{2520}$	$\frac{-2555}{2520}$	$\frac{10,405}{2520}$	$\frac{-24,875}{2520}$	$\frac{38,629}{2520}$	$\frac{-40,751}{2520}$	$\frac{29,809}{2520}$	$\frac{-15,551}{2520}$	$\frac{7129}{2520}$
	1	$\frac{-35}{2520}$	$\frac{325}{2520}$	$\frac{-1355}{2520}$	$\frac{3349}{2520}$	$\frac{-5471}{2520}$	$\frac{6289}{2520}$	$\frac{-5471}{2520}$	$\frac{4609}{2520}$	$\frac{280}{2520}$
	2	$\frac{10}{2520}$	$\frac{-95}{2520}$	$\frac{409}{2520}$	$\frac{-1061}{2520}$	$\frac{1879}{2520}$	$\frac{-2531}{2520}$	$\frac{3349}{2520}$	$\frac{595}{2520}$	$\frac{-35}{2520}$
	3	$\frac{-5}{2520}$	$\frac{49}{2520}$	$\frac{-221}{2520}$	$\frac{619}{2520}$	$\frac{-1271}{2520}$	$\frac{2509}{2520}$	$\frac{955}{2520}$	$\frac{-125}{2520}$	$\frac{10}{2520}$
	4	$\frac{4}{2520}$	$\frac{-41}{2520}$	$\frac{199}{2520}$	$\frac{-641}{2520}$	$\frac{1879}{2520}$	$\frac{1375}{2520}$	$\frac{-305}{2520}$	$\frac{55}{2520}$	$\frac{-5}{2520}$
	5	$\frac{-5}{2520}$	$\frac{55}{2520}$	$\frac{-305}{2520}$	$\frac{1375}{2520}$	$\frac{1879}{2520}$	$\frac{-641}{2520}$	$\frac{199}{2520}$	$\frac{-41}{2520}$	$\frac{4}{2520}$
	6	$\frac{10}{2520}$	$\frac{-125}{2520}$	$\frac{955}{2520}$	$\frac{2509}{2520}$	$\frac{-1271}{2520}$	$\frac{619}{2520}$	$\frac{-221}{2520}$	$\frac{49}{2520}$	$\frac{-5}{2520}$
	7	$\frac{-35}{2520}$	$\frac{325}{2520}$	$\frac{-1355}{2520}$	$\frac{3349}{2520}$	$\frac{-5471}{2520}$	$\frac{6289}{2520}$	$\frac{-5471}{2520}$	$\frac{4609}{2520}$	$\frac{280}{2520}$
	8	$\frac{280}{2520}$	$\frac{4609}{2520}$	$\frac{-5471}{2520}$	$\frac{6289}{2520}$	$\frac{-5471}{2520}$	$\frac{3349}{2520}$	$\frac{-1355}{2520}$	$\frac{325}{2520}$	$\frac{-35}{2520}$

Table 2: Linear weights  $d_k^r$  of  $(2r - 1)$ -point WENO schemes for  $r \leq 9$ .

r	k=0	k=1	k=2	k=3	k=4	k=5	k=6	k=7	k=8
1	1								
2	$\frac{1}{3}$	$\frac{2}{3}$							
3	$\frac{1}{10}$	$\frac{3}{10}$	$\frac{3}{10}$						
4	$\frac{1}{35}$	$\frac{12}{35}$	$\frac{18}{35}$	$\frac{4}{35}$					
5	$\frac{1}{126}$	$\frac{10}{126}$	$\frac{21}{126}$	$\frac{20}{126}$	$\frac{5}{126}$				
6	$\frac{1}{462}$	$\frac{7}{462}$	$\frac{25}{462}$	$\frac{100}{462}$	$\frac{25}{462}$	$\frac{1}{462}$			
7	$\frac{1}{1716}$	$\frac{286}{1716}$	$\frac{572}{1716}$	$\frac{429}{1716}$	$\frac{572}{1716}$	$\frac{186}{1716}$	$\frac{7}{1716}$		
8	$\frac{1}{6435}$	$\frac{56}{6435}$	$\frac{196}{6435}$	$\frac{392}{6435}$	$\frac{490}{6435}$	$\frac{392}{6435}$	$\frac{196}{6435}$	$\frac{8}{6435}$	
9	$\frac{1}{24,310}$	$\frac{36}{24,310}$	$\frac{504}{24,310}$	$\frac{2352}{24,310}$	$\frac{882}{24,310}$	$\frac{3528}{24,310}$	$\frac{1176}{24,310}$	$\frac{144}{24,310}$	$\frac{9}{24,310}$

Table 3: Coefficients  $a_l^r$  in the fluxes of the  $(2r - 1)$ th order upstream central linear schemes for  $r \leq 9$ .

$l$	$r = 1$	$r = 2$	$r = 3$	$r = 4$	$r = 5$	$r = 6$	$r = 7$	$r = 8$	$r = 9$
-8									$\frac{56}{12,252,240}$
-7								$\frac{-7}{360,360}$	$\frac{-1015}{12,252,240}$
-6							$\frac{30}{360,360}$	$\frac{113}{360,360}$	$\frac{8777}{12,252,240}$
-5						$\frac{-10}{27,720}$	$\frac{-425}{360,360}$	$\frac{-867}{360,360}$	$\frac{-48,343}{12,252,240}$
-4					$\frac{4}{2520}$	$\frac{122}{27,720}$	$\frac{2851}{360,360}$	$\frac{4229}{360,360}$	$\frac{191,561}{12,252,240}$
-3				$\frac{-3}{420}$	$\frac{-41}{2520}$	$\frac{-703}{27,720}$	$\frac{-12,164}{360,360}$	$\frac{-14,881}{360,360}$	$\frac{-588,127}{12,252,240}$
-2			$\frac{2}{60}$	$\frac{25}{420}$	$\frac{199}{2520}$	$\frac{2597}{27,720}$	$\frac{37,886}{360,360}$	$\frac{41,175}{360,360}$	$\frac{1,491,041}{12,252,240}$
-1		$\frac{-1}{6}$	$\frac{-13}{60}$	$\frac{-101}{420}$	$\frac{-641}{2520}$	$\frac{-7303}{27,720}$	$\frac{-97,249}{360,360}$	$\frac{-98,965}{360,360}$	$\frac{-3,409,855}{12,252,240}$
0	1	$\frac{5}{6}$	$\frac{47}{60}$	$\frac{319}{420}$	$\frac{1879}{2520}$	$\frac{20,417}{27,720}$	$\frac{263,111}{360,360}$	$\frac{261,395}{360,360}$	$\frac{8,842,385}{12,252,240}$
1		$\frac{2}{6}$	$\frac{27}{60}$	$\frac{214}{420}$	$\frac{1375}{2520}$	$\frac{15,797}{27,720}$	$\frac{211,631}{360,360}$	$\frac{216,350}{360,360}$	$\frac{7,481,025}{12,252,240}$
2			$\frac{-3}{60}$	$\frac{-38}{420}$	$\frac{-305}{2520}$	$\frac{-4003}{27,720}$	$\frac{-58,639}{360,360}$	$\frac{-63,930}{360,360}$	$\frac{-2,320,767}{12,252,240}$
3				$\frac{4}{420}$	$\frac{55}{2520}$	$\frac{947}{27,720}$	$\frac{16,436}{360,360}$	$\frac{20,154}{360,360}$	$\frac{797,985}{12,252,240}$
4					$\frac{-5}{2520}$	$\frac{-153}{27,720}$	$\frac{-3584}{360,360}$	$\frac{-5326}{360,360}$	$\frac{-241,599}{12,252,240}$
5						$\frac{12}{27,720}$	$\frac{511}{360,360}$	$\frac{1044}{360,360}$	$\frac{58,281}{12,252,240}$
6							$\frac{-35}{360,360}$	$\frac{-132}{360,360}$	$\frac{-10,263}{12,252,240}$
7								$\frac{8}{360,360}$	$\frac{1161}{12,252,240}$
8									$\frac{-63}{12,252,240}$

As  $r$  increases, the explicit formulas of  $\beta_k^{r(JS)}$  become more and more complex, which could be found in [7, 8] for  $r = 4, \dots, 9$ . These smoothness indicators can also be written in non-negative definite quadratic form[32]. By means of congruent transformation in matrix, we have

$$\beta_k^{r(JS)} = A_{k,r}^T A_{k,r}, \quad A_{k,r} = B_{k,r} \cdot (f_{i-r+k+1}, \dots, f_{i+k})^T, \quad (10)$$

where  $B_{k,r}$  is an upper triangular matrix. The expressions of  $B_{k,r}$  for  $r = 3, 4, 5$  are given in the appendix. Smoothness indicator  $\beta_k^{r(JS)}$  in this form will take  $(r^2 + r - 4)/2$  additions/subtractions and  $(r^2 + 3r - 4)/2$  multiplications as pointed out in [32], and it should be the most efficient expression for  $\beta_k^{r(JS)}$ . As for the time consuming square root computations to evaluate  $B_{k,r}$ , they will be carried out only at the beginning of the program, and hence have little effect on the time efficiency.

## 2.2 Mapped WENO schemes and Z-type WENO schemes

Henrick et al. [9] found that the fifth order WENO scheme proposed in [6] cannot achieve fifth order accuracy near some critical points and introduced a mapping procedure on the weights to overcome this problem. By using this technique the numerical dissipation is also decreased and better results are obtained at the same time. The nonlinear weights of the  $(2r - 1)$ th order mapped WENO scheme are given as

$$\omega_{M,k}^{r(JS)} = \frac{\alpha_{M,k}^r}{\sum_{l=0}^{r-1} \alpha_{M,l}^r}, \quad \alpha_{M,k}^r = g_M(\omega_k^{r(JS)}, d_k^r), \quad k = 0, 1, \dots, r, \quad (11)$$

where  $\omega_k^{r(JS)}$  are the nonlinear weights of the classical WENO scheme. And  $g_M$  is the mapping function defined as

$$g_M(\omega, C) := \frac{\omega(C + C^2 - 3C\omega + \omega^2)}{C^2 + \omega(1 - 2C)}. \quad (12)$$

Z-type WENO schemes can also obtain enhanced order of convergence at critical points and less dissipation at shocks, but with smaller computational cost than mapped WENO schemes. This kind of schemes was firstly proposed on five-point stencil[10] and was later generalized to WENO schemes on more points. In a Z-type WENO scheme, the nonlinear weights on sub-stencils are

$$\omega_k^{r(Z)} = \frac{\alpha_k^r}{\sum_{l=0}^{r-1} \alpha_l^r}, \quad \alpha_k^r = d_k^r \left( 1 + \frac{\tau_{2r-1}^p}{(\beta_k^{r(JS)})^p + \varepsilon} \right), \quad k = 0, 1, \dots, r, \quad (13)$$

where  $p$  enlarges the differences of the weights of sub-stencils and  $\varepsilon$  is the parameter avoiding zero denominator.  $\tau_{2r-1}$  can be considered as a smoothness indicator of the whole stencil and a general formula of it is[11]

$$\tau_{2r-1} = \begin{cases} |\beta_0 - \beta_{r-1}|, & \text{mod}(r, 2) = 1, \\ |\beta_0 - \beta_1 - \beta_{r-2} + \beta_{r-1}|, & \text{mod}(r, 2) = 0. \end{cases} \quad (14)$$

Note that a high order version of  $\tau_{2r-1}$  could also be found in [11]. However, there is no general formula and it will not be presented here.

## 2.3 New (2r-1)-point WENO schemes

In [14], a class of smoothness indicators  $\beta^{(S)}$  constant for sine functions was proposed, and a seven-point scheme WENO7-S was constructed using this kind of smoothness indicator. The WENO7-S scheme has both good resolution for smooth structure and good stability near discontinuities with relatively low computational cost. In this subsection, this scheme will be extended to higher order cases. First, the smoothness indicators will be introduced.

For an  $r$ -point( $r \geq 4$ ) stencil  $\{x_i, x_{i+1}, \dots, x_{i+r-1}\}$  with uniform grid length  $h$ , smoothness indicator  $\beta^{(S)}$  of  $f(x)$  can be given as

$$\beta^{(S)} = (\sigma \delta^{r-2} f)^2|_{x=x_c} + |(\sigma^2 \delta^{r-3} f)|_{x=x_c} \cdot (\delta^{r-1} f)|_{x=x_c}|, \quad (15)$$

where  $x_c = x_i + (r - 1) \cdot h/2$  is the midpoint of the stencil, and operators  $\delta, \sigma$  are defined as

$$\begin{aligned} \delta f(x) &= f(x + h/2) - f(x - h/2), \\ \sigma f(x) &= f(x + h/2) + f(x - h/2). \end{aligned} \quad (16)$$

Let

$$a = (\sigma^2 \delta^{r-3} f)|_{x=x_c}, \quad b = (\sigma \delta^{r-2} f)|_{x=x_c}, \quad c = (\delta^{r-1} f)|_{x=x_c}. \quad (17)$$



Thus, we have

$$\beta^{r(s)} = b^2 + |ac|. \quad (18)$$

And  $a, b, c$  can be represented as linear combinations of function values at the stencil points, like

$$z = \sum_{l=0}^{r-1} \alpha_{r,l} f_{i+l}. \quad (19)$$

The coefficients  $\alpha_{r,l}$  of  $a$ ,  $b$  and  $c$  for  $4 \leq r \leq 18$  are given in Table 4.

This kind of smoothness indicators has a more succinct form compared with  $\beta_k^{r(JS)}$ . Furthermore, for a sine wave  $f(x) = A \sin(kx + B) + C$  on a uniform grid with grid length  $h$ , Eq.(15) will be a value independent of  $x$ ,

$$\text{Const} = 2^{2r-2} A^2 \sin^{2r-4}(kh/2) \cos^2(kh/2). \quad (20)$$

Then, the construction technique of WENO7-S scheme will be extended to the higher order WENO schemes. For a  $(2r-1)$ -point stencil  $S = \{x_{i-r+1}, x_{i-r+2}, \dots, x_{i+r-1}\}$ , the nonlinear weights of the new  $(2r-1)$ -point ( $r \geq 5$ ) WENO scheme are

$$\omega_k^{r(S)} = \frac{\alpha_k^{r(S)}}{\sum_{k=0}^{r-1} \alpha_k^{r(S)}}, \quad \alpha_k^{r(S)} = d_k^r \left( 1 + \left( \frac{\tau_k^{2r-1(S)}}{\beta_k^{r(S)} + \varepsilon} \right) \right), \quad k = 0, 1, \dots, r-1. \quad (21)$$

$d_k^r$  are the optimal weights and  $\varepsilon$  is set as  $10^{-100}$ . Smoothness indicators  $\beta_k^{r(S)}$  on the candidate sub-stencils can be written as

$$\beta_k^{r(S)} = (\sigma \delta^{r-2} f)^2|_{x=x_{c,k}^r} + |(\sigma^2 \delta^{r-3} f)|_{x=x_{c,k}^r} \cdot (\delta^{r-1} f)|_{x=x_{c,k}^r}|, \quad k = 0, 1, \dots, r-1, \quad (22)$$

where  $x_{c,k}^r = x_i + kh - (r-1)h/2$  are the midpoints of the corresponding sub-stencils.  $\tau_k^{2r-1(S)}$  also employs this kind of smoothness indicator, but on the whole stencil.

$$\tau_k^{2r-1(S)} = (\sigma \delta^{2r-3} f)^2|_{x=x_i} + |(\sigma^2 \delta^{2r-4} f)|_{x=x_i} \cdot (\delta^{2r-2} f)|_{x=x_i}|. \quad (23)$$

The resultant WENO scheme is called as WENO(2r-1)-S scheme in this paper. The formula of  $\tau_k^{2r-1(S)}$  could also be simplified like that of WENO7-S. Let

$$c_k^r = \delta^{r-1} f|_{x=x_{c,k}^r}, \quad k = 0, 1, \dots, r-1, \quad (24)$$

which have already been obtained in the computation of  $\beta_k^{r(S)}$ . These discrete values could be extended to a function,

$$g(x) = \delta^{r-1} f(x). \quad (25)$$

Then  $\tau_k^{2r-1(S)}$  can be written as

$$\tau_k^{2r-1(S)} = (\sigma \delta^{r-2} g)^2|_{x=x_i} + |(\sigma^2 \delta^{r-3} g)|_{x=x_i} \cdot (\delta^{r-1} g)|_{x=x_i}|. \quad (26)$$

This formula is similar to Eq.(22), and the three terms in the right hand side can be obtained using Eq.(19) and Table 4.

## 2.4 Some advantages of the new WENO schemes

According to the formulas of the new WENO schemes, they should have following advantages.

1. Reducing to the linear schemes for sinusoidal waves.

For sinusoidal waves, smoothness indicators  $\beta^{r(S)}$  will be constant by design. Thus the nonlinear weights of the new WENO schemes will just equate to the optimal linear weights, and the WENO schemes become the corresponding underlying linear schemes. This means that the WENO schemes should have better performance for problem with sinusoidal space dependence. Furthermore, they will have the same approximate dispersion relation (ADR) property[35] as the corresponding underlying linear schemes. The ADR technique is a method which often be used to obtain spectral property of nonlinear schemes which relies on the extraction of a modified wavenumber from the convection of a sine wave with a certain wavenumber over a small distance. It does not mean that these WENO schemes behave the same as the underlying linear ones in smooth region, since the resultant schemes are different from the linear ones as the profile is not a monochromatic wave.

Table 4: Coefficients  $\alpha_{r,l}$  of  $a$ ,  $b$  and  $c$  in the smoothness indicators  $\beta^{r(s)}$  on  $r$ -point stencils for  $4 \leq r \leq 18$ .

$l$		0	1	2	3	4	5	6	7	8	9	10	11	12	13	14	15	16	17
$r = 4$	a	-1	-1	1	1														
	b	1	-1	-1	1														
	c	-1	3	-3	1														
$r = 5$	a	1	0	-2	0	1													
	b	-1	2	0	-2	1													
	c	1	-4	6	-4	1													
$r = 6$	a	-1	1	2	-2	-1	1												
	b	1	-3	2	2	-3	1												
	c	-1	5	-10	10	-5	1												
$r = 7$	a	1	-2	-1	4	-1	-2	1											
	b	-1	4	-5	0	5	-4	1											
	c	1	-6	15	-20	15	-6	1											
$r = 8$	a	-1	3	-1	-5	5	1	-3	1										
	b	1	-5	9	-5	-5	9	-5	1										
	c	-1	7	-21	35	-35	21	-7	1										
$r = 9$	a	1	-4	4	4	-10	4	4	-4	1									
	b	-1	6	-14	14	0	-14	14	-6	1									
	c	1	-8	28	-56	70	-56	28	-8	1									
$r = 10$	a	-1	5	-8	0	14	-14	0	8	-5	1								
	b	1	-7	20	-28	14	14	-28	20	-7	1								
	c	-1	9	-36	84	-126	126	-84	36	-9	1								
$r = 11$	a	1	-6	13	-8	-14	28	-14	-8	13	-6	1							
	b	-1	8	-27	48	-42	0	42	-48	27	-8	1							
	c	1	-10	45	-120	210	-252	210	-120	45	-10	1							
$r = 12$	a	-1	7	-19	21	6	-42	42	-6	-21	19	-7	1						
	b	1	-9	35	-75	90	-42	-42	90	-75	35	-9	1						
	c	-1	11	-55	165	-330	462	-462	330	-165	55	-11	1						
$r = 13$	a	1	-8	26	-40	15	48	-84	48	15	-40	26	-8	1					
	b	-1	10	-44	110	-165	132	0	-132	165	-110	44	-10	1					
	c	1	-12	66	-220	495	-792	924	-792	495	-220	66	-12	1					
$r = 14$	a	-1	9	-34	66	-55	-33	132	-132	33	55	-66	34	-9	1				
	b	1	-11	54	-154	275	-297	132	132	-297	275	-154	54	-11	1				
	c	-1	13	-78	286	-715	1287	-1716	1716	-1287	715	-286	78	-13	1				
$r = 15$	a	1	-10	43	-100	121	-22	-165	264	-165	-22	121	-100	43	-10	1			
	b	-1	12	-65	208	-429	572	-429	0	429	-572	429	-208	65	-12	1			
	c	1	-14	91	-364	1001	-2002	3003	-3432	3003	-2002	1001	-364	91	-14	1			
$r = 16$	a	-1	11	-53	143	-221	143	143	-429	429	-143	-143	221	-143	53	-11	1		
	b	1	-13	77	-273	637	-1001	1001	-429	-429	1001	-1001	637	-273	77	-13	1		
	c	-1	15	-105	455	-1365	3003	-5005	6435	-6435	5005	-3003	1365	-455	105	-15	1		
$r = 17$	a	1	-12	64	-196	364	-364	0	572	-858	572	0	-364	364	-196	64	-12	1	
	b	-1	14	-90	350	-910	1638	-2002	1430	0	-1430	2002	-1638	910	-350	90	-14	1	
	c	1	-16	120	-560	1820	-4368	8008	-11440	12870	-11440	8008	-4368	1820	-560	120	-16	1	
$r = 18$	a	-1	13	-76	260	-560	728	-364	-572	1430	-1430	572	364	-728	560	-260	76	-13	1
	b	1	-15	104	-440	1260	-2548	3640	-3432	1430	1430	-3432	3640	-2548	1260	-440	104	-15	1
	c	-1	17	-136	680	-2380	6188	-12376	19448	-24310	24310	-19448	12376	-6188	2380	-680	136	-17	1

Table 5: Estimations of smoothness indicators  $\beta^{r(S)}$  and  $\beta^{r(JS)}$  for  $r \geq 4$  on stencils including different kinds of points.

	Smooth points ( $n_{cp} = 0$ )	Critical points ( $n_{cp} = 1$ )	Critical points ( $n_{cp} \geq 2$ )	Discontinuous points
$\beta^{r(JS)}$	$O(h^2)$	$O(h^4)$	$O(h^{2n_{cp}+2})$	$O(1)$
$\beta^{r(S)}$	$O(h^{2r-4})$	$O(h^{2r-4})$	$O(h^{\max(2r-4, 2n_{cp}+2)})$	$O(1)$

## 2. Good behavior near critical points and discontinuous points.

By using Taylor expansion, smoothness indicators  $\beta^{r(S)}$  and  $\beta^{r(JS)}$  could be estimated as  $O(h^m)$ , where  $h$  is the grid length. Estimations of smoothness indicators  $\beta^{r(S)}$  and  $\beta^{r(JS)}$  for  $r \geq 4$  are shown in Table 5. Compared with  $\beta^{r(JS)}$ , it could be observed that the variation of  $\beta^{r(S)}$  is smaller when the stencil approaches critical points in smooth region, whereas it is larger as the stencil moves from smooth region to discontinuities. Thus,  $\beta^{r(S)}$  will do better in distinguishing discontinuous parts from smooth parts. By using smoothness indicators  $\beta^{r(S)}$ , the numerical defects near critical points like accuracy order reduction will also be alleviated. Therefore, it could be expected that the new WENO schemes will have both good resolution in smooth region and good stability near discontinuous points.

## 3. Free of power parameter $p$ .

Power parameter  $p$  in the formulation of nonlinear weights of WENO-JS and WENO-Z is removed (it equals to the case of  $p = 1$ ) for this kind of WENO schemes. This parameter is employed to enlarge the differences of the weights of candidate sub-stencils. It is suggested as an integer belong to  $[2, r]$  for the  $(2r-1)$ th order WENO-JS scheme[8]. Because of the large variation of the smoothness indicators  $\beta^{r(S)}$  near discontinuities,  $p$  could be set as 1 or be removed.

**Remark:** Supposed the parameter  $p$  is kept in the proposed method like Z-type WENO schemes. A larger  $p$  will increase the differences among the nonlinear weights of sub-stencils. So, this will not be conducive to obtaining sharp discontinuities profiles. Partly for this reason, the employment of large  $p$  is not suggested. Another is the poor stability near discontinuities for the proposed very high order schemes with large  $p$ . In the numerical experiments, obvious oscillations appear in the region of discontinuities for these schemes. Compared with the numerical results of WENO-S schemes in following sections, this oscillation is confusing. According to theoretical analysis and numerical investigations, the proposed WENO schemes have large variations of smooth indicators near discontinuities and slightly smeared discontinuities. Thus the off-centered smoother sub-stencils could obtain relatively large weights which should be even larger with the increase of  $p$ . However, the approximation values from these sub-stencils may suffer from Runge phenomenon, and which could be harmful for stability. Thus, the Runge phenomenon together with large weights of the off-centered sub-stencils may be the reason of instability near discontinuities using large  $p$ .

## 3 Time integration method and boundary treatment

A high order time method is preferred when the spatial scheme employed is a high order one. One of the most commonly used high order time methods is the third order strong stability preserving (SSP) Runge-Kutta method[33], also referred as the third order TVD Runge-Kutta method. But the spatial schemes discussed in the present paper have accuracy orders much larger than 3. If the grid size of space is very small and CFL is assigned a moderate value, the time marching error will become the major part of the error of the numerical solution in smooth region. For this case, a very high order time method should be preferred, and the linear strong stability preserving Runge-Kutta methods[36, 37] are suggested for linear problems. The third order SSP Runge-Kutta method and the linear strong stability preserving Runge-Kutta methods will be described in the first two subsections. As for the boundary treatment, it is discussed in the last subsection.

### 3.1 The third order SSP Runge-Kutta method

This third order SSP Runge-Kutta method[33] can be written as

$$\begin{aligned} u^{(1)} &= u^n + \Delta t L(u^n), \\ u^{(2)} &= \frac{3}{4}u^n + \frac{1}{4}u^{(1)} + \frac{1}{4}\Delta t L(u^{(1)}), \\ u^{n+1} &= \frac{1}{3}u^n + \frac{2}{3}u^{(2)} + \frac{2}{3}\Delta t L(u^{(2)}), \end{aligned} \quad (27)$$

where  $L(u)$  is a discretization of the spatial operator.

Table 6: Coefficients  $\alpha_{m,j}$  of SSP Linear  $(m, m-1)$  Runge-Kutta methods for  $2 \leq m \leq 10$ .

Stages $m$	$\alpha_{m,0}$	$\alpha_{m,1}$	$\alpha_{m,2}$	$\alpha_{m,3}$	$\alpha_{m,4}$	$\alpha_{m,5}$	$\alpha_{m,6}$	$\alpha_{m,7}$	$\alpha_{m,8}$	$\alpha_{m,9}$
2	0	1								
3	$\frac{1}{3}$	0	$\frac{2}{3}$							
4	0	$\frac{2}{3}$	0	$\frac{1}{3}$						
5	$\frac{1}{5}$	0	$\frac{2}{3}$	0	$\frac{2}{15}$					
6	$\frac{1}{9}$	$\frac{2}{5}$	0	$\frac{4}{9}$	0	$\frac{2}{45}$				
7	$\frac{1}{7}$	$\frac{2}{9}$	$\frac{2}{5}$	0	$\frac{2}{9}$	0	$\frac{4}{315}$			
8	$\frac{2}{15}$	$\frac{2}{7}$	$\frac{2}{9}$	$\frac{4}{15}$	0	$\frac{4}{45}$	0	$\frac{1}{315}$		
9	$\frac{11}{81}$	$\frac{4}{15}$	$\frac{2}{7}$	$\frac{4}{27}$	$\frac{2}{15}$	0	$\frac{4}{135}$	0	$\frac{2}{2835}$	
10	$\frac{71}{525}$	$\frac{22}{81}$	$\frac{4}{15}$	$\frac{4}{21}$	$\frac{2}{27}$	$\frac{4}{75}$	0	$\frac{8}{945}$	0	$\frac{2}{14175}$

Table 7: Coefficients  $\alpha_{m,j}$  of SSP Linear  $(m, m-1)$  Runge-Kutta methods for  $m = 12, 14, 16, 18$ .

Stages $m$	$\alpha_{m,0}$	$\alpha_{m,1}$	$\alpha_{m,2}$	$\alpha_{m,3}$	$\alpha_{m,4}$	$\alpha_{m,5}$	$\alpha_{m,6}$	$\alpha_{m,7}$	$\alpha_{m,8}$
12	$\frac{1151}{8505}$	$\frac{134}{495}$	$\frac{142}{525}$	$\frac{44}{243}$	$\frac{4}{45}$	$\frac{4}{105}$	$\frac{4}{405}$	$\frac{8}{1575}$	0
14	$\frac{29,543}{218,295}$	$\frac{5542}{20,475}$	$\frac{2302}{8505}$	$\frac{268}{1485}$	$\frac{142}{1575}$	$\frac{44}{1215}$	$\frac{8}{675}$	$\frac{2}{2205}$	$\frac{2}{2835}$
16	$\frac{274,328}{2,027,025}$	$\frac{172,654}{637,875}$	$\frac{59,086}{218,295}$	$\frac{11,084}{61,425}$	$\frac{2,302}{25,515}$	$\frac{268}{7425}$	$\frac{284}{23,625}$	$\frac{88}{25,515}$	$\frac{4}{4725}$
18	$\frac{111,102,841}{820,945,125}$	$\frac{15,066,938}{55,665,225}$	$\frac{548,656}{2,027,025}$	$\frac{345,308}{1,913,625}$	$\frac{59,086}{654,885}$	$\frac{11,084}{307,125}$	$\frac{4604}{382,725}$	$\frac{536}{155,925}$	$\frac{142}{165,375}$
Stages $m$	$\alpha_{m,9}$	$\alpha_{m,10}$	$\alpha_{m,11}$	$\alpha_{m,12}$	$\alpha_{m,13}$	$\alpha_{m,14}$	$\alpha_{m,15}$	$\alpha_{m,16}$	$\alpha_{m,17}$
12	$\frac{4}{8505}$	0	$\frac{2}{467,775}$						
14	$\frac{4}{14,175}$	0	$\frac{8}{467,775}$	0	$\frac{2}{42,567,525}$				
16	$\frac{4}{19,845}$	$\frac{4}{127,575}$	$\frac{8}{779,625}$	0	$\frac{8}{18,243,225}$	0	$\frac{1}{638,512,875}$		
18	$\frac{44}{229,635}$	$\frac{8}{212,625}$	$\frac{8}{1,091,475}$	$\frac{4}{4,209,975}$	$\frac{8}{30,405,375}$	0	$\frac{16}{1,915,538,625}$	0	$\frac{2}{97,692,469,875}$

The proposed high order WENO schemes coupled with this third order Runge-Kutta time discretization, are linearly stable under CFL numbers between 1.24 and 0.91 for  $r = 4$  to 9. However, to obtain essentially non-oscillatory results near discontinuities, smaller CFL numbers are required[7]. According to our numerical experiments of an advection of a square wave, to obtain results without apparent undershooting and overshooting, CFL numbers for WENO(2r-1)-S should be less than 0.59, 0.54, 0.49, 0.41, 0.33, 0.29 for  $r = 4, \dots, 9$  respectively.

### 3.2 The SSP linear Runge-Kutta methods

For very high order WENO schemes, it should be better to apply time methods with the same order. Like the work in [8], the strong stability preserving (SSP) linear Runge-Kutta methods  $lSSPRK(m, m-1)$  proposed in [36, 37] could be employed as the time integration method. Here the two parameters in the brackets of  $lSSPRK(m, m-1)$  mean  $m$  stage and order  $p = m-1$ . This kind of time integration method doubles the CFL number of the explicit forward Euler method. The formulas of  $lSSPRK(m, m-1)$  are

$$\begin{aligned}
u^{(0)} &= u^n, \\
u^{(i)} &= u^{(i-1)} + \frac{1}{2} \Delta t L(u^{(i-1)}), \quad i = 1, \dots, m-1, \\
u^{n+1} &= \sum_{k=0}^{m-2} \alpha_{m,k} u^{(k)} + \alpha_{m,m-1} (u^{(m-1)} + \frac{1}{2} \Delta t L(u^{(m-1)})),
\end{aligned} \tag{28}$$

where the coefficients  $\alpha_{m,j}$  are given recursively by:

$$\begin{aligned}
\alpha_{2,0} &= 0, \quad \alpha_{2,1} = 1 \\
\alpha_{m,k} &= \frac{2}{k} \alpha_{m-1,k-1}, \quad k = 1, \dots, m-2, \\
\alpha_{m,m-1} &= \frac{2}{m} \alpha_{m-1,m-2}, \quad \alpha_{m,0} = 1 - \sum_{k=1}^{m-1} \alpha_{m,k}.
\end{aligned} \tag{29}$$

The values of  $\alpha_{m,j}$  are listed in Table 6 for  $m = 2, 3, \dots, 10$ , and in Table 7 for  $m = 12, 14, 16, 18$ .

As pointed out by Balsara and Shu[7], higher order Runge-Kutta time methods allow larger CFL numbers for linear stability. To obtain results without apparent undershooting and overshooting for square wave, the largest CFL numbers fall between 1.49 and 0.83 for WENO(2r-1)-S schemes combined with  $lSSPRK(2r, 2r-1)$  for  $r = 4$  to 9. Although large CFL numbers are allowed, this kind of time method needs more computing

time than the third order Runge-Kutta method. The reason is that it takes  $2r$  stages in one Runge-Kutta procedure, versus 3 stages of the third order Runge-Kutta method. Furthermore, it can obtain very high order of accuracy only for linear problems. In this paper, the  $l$ SSPRK( $2r, 2r - 1$ ) methods will be implemented in the numerical tests only for one-dimensional linear problems.

### 3.3 Boundary treatment

In the vicinity of the boundaries, there are not enough node points to construct the numerical flux of a high order scheme. In the present study, ghost node points are employed and the flux can be evaluated by using the same formula as inner points. Then the problem is how to assign values to these ghost points. For periodic boundary, these values could be obtained from the node values in the other side of this boundary. For inflow condition, the exact values are given for these ghost points. As for outflow, these values can be obtained by extrapolation. Since very high order extrapolation may lead to large error, a third order extrapolation is implemented in the current work. For subsonic boundaries of Euler equations, a local characteristic decomposition method is employed. The characteristic variables on these node points will be obtained by inflow or outflow condition according to the sign of the characteristic speed. Then these characteristic variables will be projected back to the variables in the form needed. As for inviscid wall, the reflecting boundary treatment is employed.

## 4 Convergence rates of the new WENO schemes

### 4.1 Theoretical analysis

Following is the necessary and sufficient conditions on the weights for the  $(2r - 1)$ -point WENO scheme to achieve the formal  $(2r - 1)$ th order of convergence at smooth parts of the solution[11]:

$$\sum_{k=0}^{r-1} A_k(\omega_k^+ - \omega_k^-) = O(h^r), \quad \omega_k^\pm - d_k^r = O(h^{r-1}), \quad k = 0, 1, \dots, r-1. \quad (30)$$

And a sufficient condition can be given as

$$\omega_k^\pm - d_k^r = O(h^r), \quad k = 0, 1, \dots, r-1. \quad (31)$$

However, in practice, if the second equation of Eq.(30) is satisfied, the scheme will usually be  $(2r - 1)$ th order accurate. The reason is that the coefficient of the lowest order term in Taylor expansions is usually differentiable. Then the difference in Eq.(2) would give an extra  $O(h)$ , and cancel the one in the denominator.

For a stencil centered at  $x_i$ , the Taylor expansion of  $\tau^{2r-1(S)}$  in Eq.(23) will be

$$\tau^{2r-1(S)} = 4 \left[ (f_i^{(2r-3)})^2 + |f_i^{(2r-4)} \cdot f_i^{(2r-2)}| \right] h^{4r-6} + O(h^{4r-5}). \quad (32)$$

For the smoothness indicators on the candidate sub-stencils,

$$\beta_k^{r(S)} = 4 \left[ (f_i^{(r-2)})^2 + |f_i^{(r-3)} \cdot f_i^{(r-1)}| \right] h^{2r-4} + O(h^{2r-3}). \quad (33)$$

If  $f^{(r-2)} = O(1)$  or  $f^{(r-3)} \cdot f^{(r-1)} = O(1)$ , we have

$$\alpha_k^r = d_k^r \left( 1 + \frac{\tau^{2r-1(S)}}{\beta_k^{r(S)}} \right) = d_k^r + O(h^{2r-2}). \quad (34)$$

Then

$$\omega_k^{r(S)} - d_k^r = O(h^{2r-2}). \quad (35)$$

The sufficient condition (31) is satisfied and the WENO( $2r-1$ )-S scheme is  $(2r - 1)$ th order accurate for  $r \geq 4$ . However, degradation of the convergence order may happen if the assumption is not satisfied, and this will be discussed below.

Since the convergence result of  $r = 4$  has been given in [14], thus the case of  $r \geq 5$  is considered. Note that the first derivative does not appear in both expansion forms of  $\tau^{2r-1(S)}$  and  $\beta_k^{r(S)}$  for  $r \geq 5$ . So, degradation of the convergence order is irrelevant to the critical points, whereas it can only appear at points where  $f^{(r-2)} = 0$  and  $f^{(r-3)} \cdot f^{(r-1)} = 0$ . Then the accuracy order is discussed according to whether  $f^{(r-3)}$  equals to zero or not.

(a) If  $f^{(r-3)} \neq 0$ , only those points where  $f^{(r-2)} = f^{(r-1)} = \dots = f^{(r_m)} = 0$  need be considered, where  $r_m \geq r - 2$ . Then

$$\beta_k^{(S)} = C_{k,r_m+1} f^{(r-3)} f^{(r_m+1)} h^{r+r_m-2} + O(h^{r+r_m-1}), \quad (36)$$

$$\tau^{2r-1(S)} = C_\tau h^l + O(h^{l+1}), \quad l = \max(4r - 6, 2r_m + 2), \quad (37)$$

where  $C_{k,r_m+1}$  and  $C_\tau$  are nonzero values independent of  $h$ . Then

$$\frac{\tau^{2r-1(S)}}{\beta_k^{r(S)}} = O(h^{l-r-r_m+2}). \quad (38)$$

The sufficient condition (31) will become

$$l - r - r_m + 2 \geq r. \quad (39)$$

It can be proved that this inequality always holds true. Therefore, the sufficient condition is satisfied and the accuracy order of the scheme will be preserved.

(b) If  $f^{(r-3)} = 0$ , the degradation may happen for the case  $f^{(r-3)} = f^{(r-2)} = \dots = f^{(r_m)} = 0$ , where  $r_m$  need be determined. In the vicinity of these points,

$$\beta_k^{r(S)} = C_{k,r_m+1} (f^{(r_m+1)})^2 h^{2r_m+2} + O(h^{2r_m+3}), \quad (40)$$

$$\tau^{2r-1(S)} = C_\tau h^l + O(h^{l+1}), \quad l = \max(4r - 6, 2r_m + 2), \quad (41)$$

where  $C_{k,r_m+1}$  and  $C_\tau$  are nonzero values independent of  $h$ . And then

$$\frac{\tau^{2r-1(S)}}{\beta_k^{r(S)}} = O(h^{l-2r_m-2}). \quad (42)$$

So, the sufficient condition (31) requires

$$l - 2r_m - 2 \geq r. \quad (43)$$

Therefore, a sufficient condition for  $(2r - 1)$ th order accurate is

$$r_m \leq 3r/2 - 4. \quad (44)$$

And a relaxed condition which is often effective could be obtained by replacing the sufficient condition Eq.(31) with the second equation of Eq.(30).

$$r_m \leq 3r/2 - 7/2.$$

Therefore, for the WENO(2r-1)-S scheme with  $r \geq 5$ , degradation of accuracy order may only happen near those points satisfied  $f^{(r-3)} = f^{(r-2)} = \dots = f^{(r_m)} = 0$ , where  $r_m > 3r/2 - 4$ .

## 4.2 Numerical validation of accuracy order

To validate the convergence order of these new WENO schemes, linear advection equation with periodic boundary condition is used for test. The initial problem is

$$\begin{cases} \frac{\partial u}{\partial t} + \frac{\partial u}{\partial x} = 0, & -1 \leq x \leq 1. \\ u(x, 0) = u_0(x), \end{cases} \quad (45)$$

where  $u_0(x)$  is periodic. Like the work in [8], *lssprk*(2r, 2r - 1) is employed as the time integration method for WENO(2r-1)-S. Because very small error will appear in the numerical tests of accuracy order, the 128-bit quadruple precision floating point is implemented for this kind of numerical validations. And the double precision is implemented for other kinds of numerical tests in this paper.

Firstly, the initial condition is  $u_0(x) = \sin(\pi x - \sin(\pi x)/\pi)$  and the end time is 2. The  $L_1$ ,  $L_\infty$  errors and the corresponding orders of accuracy are shown in Table 8. Obviously, the designed convergence rates are achieved.

Then the initial function is replaced with  $\sin^4(\pi x)$ , for which  $x = 0$  is a critical point with  $n_{cp} = 3$ . According to the previous analysis, WENO(2r-1)-S schemes ( $r \geq 5$ ) will maintain the optimal accuracy order in the vicinity of these points. The numerical convergence orders given in Table 9 validate the analysis.

Table 8: Convergence orders of the new  $(2r - 1)$ -point WENO schemes for initial profile  $u_0(x) = \sin(\pi x - \sin(\pi x)/\pi)$  with  $t = 2$ .

N	$L_1$ error	$L_1$ order	$L_\infty$ error	$L_\infty$ order
$r = 5$				
20	2.262E-04		3.751E-04	
40	3.366E-07	9.393	4.642E-07	9.658
80	8.946E-10	8.556	2.767E-09	7.390
160	1.193E-12	9.551	1.957E-12	10.465
$r = 6$				
20	2.535E-05		3.947E-05	
40	2.044E-08	10.277	3.487E-08	10.145
80	1.105E-11	10.853	1.938E-11	10.813
160	5.533E-15	10.963	9.770E-15	10.954
$r = 7$				
20	7.084E-06		1.123E-05	
40	1.846E-09	11.906	3.231E-09	11.763
80	2.683E-13	12.748	4.865E-13	12.697
160	3.403E-17	12.945	6.260E-17	12.924
$r = 8$				
20	2.104E-06		2.854E-06	
40	2.081E-10	13.304	3.613E-10	12.948
80	7.936E-15	14.679	1.511E-14	14.545
160	2.565E-19	14.917	4.970E-19	14.892
$r = 9$				
20	1.890E-06		2.122E-06	
40	2.767E-11	16.060	5.114E-11	15.341
80	2.868E-16	16.558	5.707E-16	16.451
160	2.374E-21	16.882	4.747E-21	16.875

Table 9: Convergence orders of the new  $(2r - 1)$ -point WENO schemes for initial profile  $u_0(x) = \sin^4(\pi x)$  with  $t = 2$ .

N	$L_1$ error	$L_1$ order	$L_\infty$ error	$L_\infty$ order
$r = 5$				
20	1.913E-02		1.724E-02	
40	4.063E-05	8.879	3.468E-05	8.957
80	9.243E-08	8.780	7.409E-08	8.871
160	1.836E-10	8.976	1.442E-10	9.005
$r = 6$				
20	6.722E-03		5.321E-03	
40	3.658E-06	10.844	2.910E-06	10.836
80	2.050E-09	10.801	1.589E-09	10.839
160	1.027E-12	10.962	8.048E-13	10.947
$r = 7$				
20	2.375E-03		2.022E-03	
40	3.193E-07	12.861	2.604E-07	12.923
80	4.632E-11	12.751	3.585E-11	12.826
160	5.839E-15	12.954	4.570E-15	12.938
$r = 8$				
20	7.463E-04		6.351E-04	
40	2.852E-08	14.676	2.210E-08	14.811
80	1.058E-12	14.718	8.188E-13	14.720
160	3.355E-17	14.945	2.625E-17	14.929
$r = 9$				
20	2.236E-04		1.945E-04	
40	2.559E-09	16.415	1.989E-09	16.577
80	2.438E-14	16.680	1.886E-14	16.687
160	1.944E-19	16.936	1.521E-19	16.920

Table 10: Convergence orders of the new  $(2r - 1)$ -point WENO schemes for inviscid Burgers equation with  $t = 0.1$ .

N	$L_1$ error	$L_1$ order	$L_\infty$ error	$L_\infty$ order
$r = 5$				
40	4.957E-07		2.326E-06	
80	1.205E-09	8.685	6.364E-09	8.514
160	2.240E-12	9.071	1.197E-11	9.055
320	4.044E-15	9.114	2.177E-14	9.102
$r = 6$				
40	1.576E-07		9.221E-07	
80	1.495E-10	10.042	8.217E-10	10.132
160	7.453E-14	10.970	4.579E-13	10.809
320	3.362E-17	11.114	2.089E-16	11.098
$r = 7$				
40	6.528E-08		2.569E-07	
80	2.505E-11	11.348	1.573E-10	10.673
160	3.751E-15	12.705	2.495E-14	12.622
320	4.325E-19	13.082	3.008E-18	13.018
$r = 8$				
40	2.120E-08		5.205E-08	
80	6.242E-12	11.730	3.986E-11	10.351
160	2.617E-16	14.542	1.945E-15	14.323
320	7.971E-21	15.002	6.017E-20	14.980
$r = 9$				
40	1.168E-08		2.994E-08	
80	1.717E-12	12.732	1.282E-11	11.189
160	2.451E-17	16.096	1.942E-16	16.011
320	1.979E-22	16.918	1.614E-21	16.877

At last, the inviscid Burgers equation which is a nonlinear one is under consideration. The initial value problem is

$$\begin{cases} \frac{\partial u}{\partial t} + \frac{\partial(u^2)}{\partial x} = 0, & -1 \leq x \leq 1. \\ u(x, 0) = 0.5 + \sin(\pi x). \end{cases}$$

Periodic boundary is implemented here. The end time is  $t = 0.1$  which is less than  $1/\pi$  when the shock will generate. Thus, the result is still smooth. In this test, the fourth order Runge-Kutta method[6] is employed instead of  $lssprk(2r, 2r - 1)$  because they are only second order accurate for nonlinear problems. For WENO(2r-1)-S scheme, as the grid length is halved the time step will be multiplied by  $2^{-(2r-1)/4}$ . Thus, the error caused by the time method will be  $O(h^{2r-1})$ . The global Lax-Friedrichs splitting is used because both positive and negative characteristic speed could exist for this problem. The results are given in Table 10, and it is validated again that the desired accuracy orders are achieved.

## 5 Computational efficiency

### 5.1 Floating point operations for one smoothness indicator

The computational efficiency could be analyzed by counting the floating points operations. The classical smoothness indicator  $\beta^{r(JS)}$  takes  $r^2 + 2r - 4$  floating point operations in the form of summation of perfect squares[32]. However,  $\beta^{r(S)}$  takes only  $6r - 5$  floating point operations which grows linearly with  $r$ . The counts of floating point operations on  $r$ -point ( $r = 4, 5, \dots, 9$ ) stencil for these two kinds of smoothness indicators are listed in Table 11. Obviously  $\beta^{r(S)}$  requires less floating point operations, especially for large  $r$ .

**Remark:** To obtain the value of  $\beta^{r(S)}$ , it requires  $3r - 2$  addition/subtraction operations and  $3r - 4$  multiplications and one absolute value function. The count of multiplications is  $3r - 4$  instead of  $3r + 2$  because both the first and the last coefficients of  $\sigma \delta^{n-2} f|_{x=x_c}$ ,  $\sigma^2 \delta^{n-3} f|_{x=x_c}$  and  $\delta^{n-1} f|_{x=x_c}$  are 1 or  $-1$ . For any of



Table 11: Counts of different kinds of floating point operations to obtain a smoothness indicator,  $\beta^{r(JS)}$  and  $\beta^{r(S)}$ .

Counts of operations	Additions/subtractions		Multiplications		Absolute value operation		Total	
	$\beta^{r(JS)}$	$\beta^{r(S)}$	$\beta^{r(JS)}$	$\beta^{r(S)}$	$\beta^{r(JS)}$	$\beta^{r(S)}$	$\beta^{r(JS)}$	$\beta^{r(S)}$
$r = 4$	8	10	12	4	0	1	20	15
$r = 5$	13	10	18	8	0	1	31	19
$r = 6$	19	16	25	12	0	1	44	29
$r = 7$	26	18	33	14	0	1	59	33
$r = 8$	34	22	42	18	0	1	76	41
$r = 9$	43	24	52	22	0	1	95	47

the other coefficients for these three terms, every 1 or  $-1$  will decrease one multiplication and every zero will decrease one multiplication and one addition/subtraction. Therefore the total counts listed in Table 11 for  $\beta^{r(S)}$  may be less than  $6r - 5$ .

## 5.2 Computational efficiency of the new WENO schemes

In the previous subsection, smoothness indicator  $\beta^{r(S)}$  is shown to be taken fewer floating point operations than the classical one. Moreover, for  $(2r - 1)$ -point WENO scheme,  $\beta^{r(S)}$  needs be computed on  $r$  different candidate sub-stencils. Then, there exists other efficient ways to compute these  $r$  smoothness indicators which could further raise the computational efficiency of the corresponding  $(2r - 1)$ -point WENO scheme.

Note that the components  $\sigma^2 \delta^{r-3} f$ ,  $\sigma \delta^{r-2} f$  and  $\delta^{r-1} f$  of  $\beta^{r(S)}$  can be computed only by using addition and subtraction. At first, the first to the  $(r - 1)$ th undivided differences in the stencil can be calculated successively. As all these differences are obtained, the three components could be calculated with 2, 1 and 0 extra additions respectively. Furthermore, to obtain the  $r$  smoothness indicators on the candidate sub-stencils of WENO(2r-1)-S scheme, the first to the  $(r - 1)$ th differences will take  $3r^2/2 - 5r/2 + 1$  subtractions, and the remain operations include  $4r$  additions/subtractions,  $2r$  multiplications and  $r$  absolute value operations. The count of floating point operations is  $3r^2/2 + 9r/2 + 1$  which is less than the original value  $r(6r - 5)$  obtained from directly using the computing way of the previous subsection. Moreover, only  $2r$  multiplications are needed for this computation method versus  $r(3r - 4)$  of the direct method. However, this computational method is less efficient on our X86 computing devices than the direct method which should be attributed to the following reasons. One is that there is no significant difference between the computational costs of one addition/subtraction and one multiplication for recent X86 CPUs. Secondly, the procedure calculating the first to the  $(r - 1)$ th differences successively may not be effective for these CPUs. And the additional intermediate variables needed may reduce the computational efficiency. Nonetheless this method should be more efficient on those computational devices where one addition/subtraction consumes much less time than one multiplication.

According to the second reason, the intermediate variables should be reduced to improve efficiency. Note that  $\sigma^2 \delta^{r-3} f$ ,  $\sigma \delta^{r-2} f$  and  $\delta^{r-1} f$  could be represented by the  $(r - 3)$ th undivided differences in a simple form. Assuming each of the  $(r - 3)$ th differences is computed directly, which means only  $r + 2$  additional variables are needed. According to the numerical experiments, this approach is more efficient than the direct method for  $r \geq 5$ . Let

$$g_l = \delta^{r-3} f|_{x=x_c+lh-(r+1)h/2}, \quad l = 0, 1, \dots, r + 1, \quad (46)$$

where  $x_c$  is the midpoint of the whole stencil. It can be extended to a function as

$$g_l = g(x_c + lh - (r + 1)h/2).$$

Thus,

$$\beta_k^{r(S)} = (\sigma \delta g)^2|_{x=x_{c,k}^r} + \left| (\sigma^2 g)|_{x=x_{c,k}^r} \cdot (\delta^2 g)|_{x=x_{c,k}^r} \right|.$$

The explicit expression will be

$$\beta_k^{r(S)} = (-g_k + g_{k+2})^2 + |(g_k + 2g_{k+1} + g_{k+2}) \cdot (g_k - 2g_{k+1} + g_{k+2})|, \quad k = 0, 1, \dots, r - 1. \quad (47)$$

Then the algorithm of computing the smoothness indicators  $\beta_k^{r(S)}$  and the  $\tau^{2r-1(S)}$  for the  $(2r-1)$ -point stencil  $S = \{x_{i-r+1}, x_{i-r+2}, \dots, x_{i+r-1}\}$  will be given as:

1. Compute all the  $(r - 3)$ th undivided differences in the  $(2r - 1)$ -point stencil,

$$\theta_j = \sum_{s=0}^{r-3} \alpha_{r-2,s} f_{i-r+s+j+1}, \quad 0 \leq j \leq r + 1,$$

Table 12: Counts of different kinds of floating point operations in a  $(2r - 1)$ -point WENO procedure. Schemes: WENO-S, WENO-JS and FWENO.

Counts of operations	Additions/subtractions	Multiplications	Divisions	Absolute value operations	Total
$\beta_k^{r(S)}$ (WENO-S)	$r^2 + 5r - 6$	$r^2 + 2r - 8$	0	$r$	$2r^2 + 7r - 14$
$\tau^{2r-1(S)}$ (WENO-S)	$3r - 2$	$3r - 4$	0	1	$6r - 5$
Others(WENO-S)	$r^2 + 3r - 2$	$r^2 + 3r$	$r + 1$	0	$2r^2 + 7r - 1$
SUM(WENO-S)	$2r^2 + 11r - 10$	$2r^2 + 7r - 12$	$r + 1$	$r + 1$	$4r^2 + 20r - 20$
SUM(WENO-JS)	$(r^3 + 3r^2 - 4)/2$	$(r^3 + 5r^2 + 2r)/2$	$r + 1$	0	$r^3 + 4r^2 + 2r - 1$
SUM(FWENO)	$r^2 + 10r - 10$	$2r^2 + 5r - 2$	$r + 1$	0	$3r^2 + 17r - 11$

where coefficients  $\alpha_{r-2,s}$  are parameters  $c$  for  $(r - 2)$ -point stencil in Table 4.

2. Compute  $a_k, b_k$  and  $c_k$ ,

$$a_k = \theta_k + 2\theta_{k+1} + \theta_{k+2}, \quad b_k = -\theta_k + \theta_{k+2}, \quad c_k = \theta_k - 2\theta_{k+1} + \theta_{k+2}, \quad 0 \leq k \leq r - 1.$$

3. Compute  $\beta_k^{r(S)}$ ,

$$\beta_k^{r(S)} = b_k^2 + |a_k c_k|, \quad 0 \leq k \leq r - 1.$$

4. Compute  $a^\tau, b^\tau$  and  $c^\tau$  by using formula

$$z^\tau = \sum_{k=0}^{r-1} \alpha_{r,k} c_k, \quad 0 \leq k \leq r - 1,$$

where  $\alpha_{r,k}$  of  $a^\tau, b^\tau$  and  $c^\tau$  are parameters  $a, b$  and  $c$  for  $r$ -point stencil in Table 4 respectively.

5. Compute  $\tau^{2r-1(S)}$ ,

$$\tau^{2r-1(S)} = (b^\tau)^2 + |a^\tau c^\tau|.$$

The counts of floating point operations in one  $(2r - 1)$ -point WENO procedure for  $r \geq 5$  will be considered now. Table 12 shows these numbers in a WENO(2r-1)-S procedure. As for comparison, the operations needed for WENO-JS and the Fast WENO(abbreviated as FWENO) schemes[32] are also given in this table. Here the WENO-JS schemes employ  $p = 2$ , and this value may lead to oscillations near discontinuities which is suggested as  $p \in [2, r]$  in [8]. In the FWENO schemes, the suggested values  $s_1 = r/2$  and  $s_2 = 1$  are employed. It could be observed from the table that the counts of operations of WENO-S and FWENO increase quadratically with respect to  $r$ , whereas the number of those of WENO-JS is cubic. Then the operations for these schemes with  $5 \leq r \leq 9$  are shown in Fig.1. In this figure, it could be observed that FWENO schemes require the fewest operations, followed by WENO-S and WENO-JS schemes. However, there are some problems when using very high order FWENO schemes which will be shown in the numerical tests.

An advection of a sine function is used to test the time efficiency. This initial value problem is defined as

$$\begin{cases} \frac{\partial u(x,t)}{\partial t} + \frac{\partial u(x,t)}{\partial x} = 0, \\ u(x,0) = \sin(\pi x). \end{cases}$$

The computational area is  $[-1, 1]$  and the periodic boundary is employed. CFL is set as 0.5 and the third order SSP Runge-Kutta is taken as the time advancing method. A uniform grid is employed whose number of node points is  $N = 10000$ . These computations are carried out on a computer with AMD Ryzen 7 2700X@3GHz using a FORTRAN code. The elapsed time that the wave is advected for a whole period, which corresponds to  $t = 2$ , is recorded. The results are shown in Table 13, and the relative values to the corresponding time of WENO-JS are also tabulated in. According to this table, WENO-S schemes require only about 50% to 75% CPU time of those of WENO-JS schemes for  $r = 5, \dots, 9$ , but they are slower than FWENO schemes. Note that WENO-JS schemes in this table do not employ the mapping procedure which also needs some calculations.

Figure 1: Counts of floating point operations in a  $(2r - 1)$ -point WENO procedure. Schemes: WENO-S, WENO-JS and FWENO.

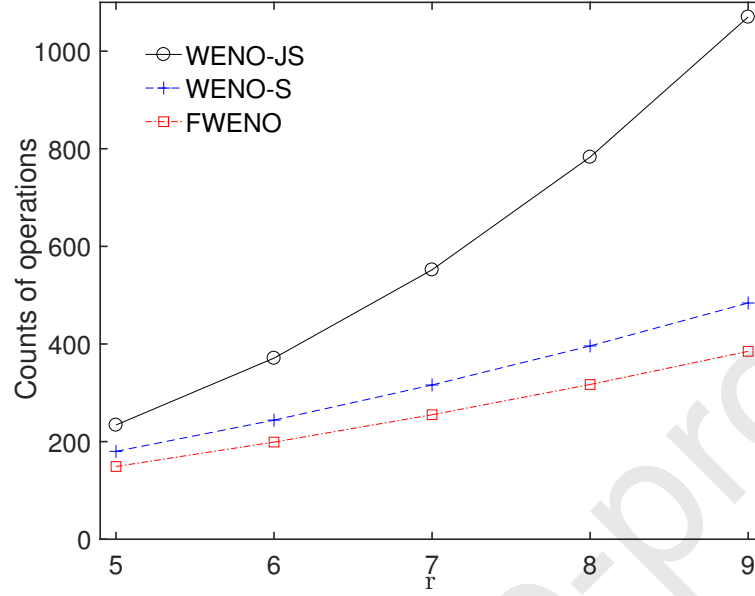


Table 13: Elapsed time for advection of a sine function using  $(2r - 1)$ -point WENO-JS, WENO-S and FWENO schemes.

Schemes		r=5	r=6	r=7	r=8	r=9
WENO-JS	Time(s)	33.290	49.858	71.136	95.322	141.04
WENO-S	Time(s)	25.209	36.855	49.280	48.938	70.091
	Relative value	0.757	0.739	0.693	0.513	0.497
FWENO	Time(s)	22.136	28.377	43.212	41.278	61.668
	Relative value	0.665	0.569	0.607	0.433	0.437

**Remark:** In this numerical test, WENO13-S ( $r = 7$ ) consumes even larger time than WENO15-S ( $r = 8$ ), which also happens for FWENO. This should be attributed to the memory alignment. As  $r = 8 = 2^3$ , there are some arrays in the program with dimension  $2^3$ , which should be helpful for the time efficiency of the program. However, the elapsed time of WENO-JS increases monotonically over  $r$ . The reason should be that the increased floating point operations for smoothness indicators of WENO-JS have a greater impact on efficiency than memory alignment.

## 6 Numerical tests for 1D scalar problems

In this section, the proposed WENO schemes, termed as WENO-S are tested for some one-dimensional scalar problems. The mapped very high order WENO schemes, termed as WENO-M here[8], and FWENO schemes[32] join the test for comparison. The parameter  $\varepsilon$  avoiding zero denominator is set as  $10^{-100}$  for all the WENO schemes. The power parameter  $p = r$  is employed for the WENO(2r-1)-M scheme. The (2r-1)th order WENO-S, WENO-M, FWENO schemes are denoted as WENO(2r-1)-S, WENO(2r-1)-M and FWENO(2r-1) respectively. In this section, the  $l$ SSPRK( $2r, 2r - 1$ ) schemes are implemented as the time integration methods.

(1) First, we consider an advection of four kinds of waves proposed in [6]. The initial value problem is

$$\begin{cases} \frac{\partial u}{\partial t} + \frac{\partial u}{\partial x} = 0, & -1 \leq x \leq 1. \\ u(x, 0) = u_0(x). \end{cases} \quad (48)$$

The initial condition of this linear advection test is

$$u_0(x) = \begin{cases} \frac{1}{6}[G(x, \beta, z - \delta) + 4G(x, \beta, z) + G(x, \beta, z + \delta)], & x \in [-0.8, -0.6], \\ 1, & x \in [-0.4, -0.2], \\ 1 - |10(x - 0.1)|, & x \in [0, 0.2], \\ \frac{1}{6}[F(x, \alpha, a - \delta) + 4F(x, \alpha, a) + F(x, \alpha, a + \delta)], & x \in [0.4, 0.6], \\ 0, & \text{otherwise,} \end{cases} \quad (49)$$

where

$$G(x, \beta, z) = e^{-\beta(x-z)^2}, \quad F(x, \alpha, a) = \sqrt{\max(1 - \alpha^2(x - a)^2, 0)},$$

with  $z = -0.7$ ,  $\delta = 0.005$ ,  $\beta = (\log 2)/(36\delta^2)$ ,  $a = 0.5$  and  $\alpha = 10$ . Thus, it is composed of a Gaussian wave, a square wave, a triangle wave and an elliptic wave. The periodic boundary is imposed for this problem.

At first, the end time is set as  $t = 8$  and the number of mesh points is  $N = 200$ . CFL number is set as 0.5. The results of WENO-S schemes are shown in Fig.2a. It could be observed there are no visible oscillations in all these results. As expected, the results become closer to the exact solution with the increase of  $r$ . WENO9-S obtains an undershooting with a minimum value about  $-0.01$  near  $x = 0.2$ , and WENO15-S obtains a undershooting with a minimum value about  $-0.003$  near  $x = 0$ . As for others, no visible overshooting(or undershooting) could be found. The results of WENO-M schemes are shown in Fig.2b. In this figure, no visible oscillation or overshooting(or undershooting) appears in these results. However, they are worse than the corresponding results of WENO-S schemes which could be viewed in the regions of square wave and elliptic wave. Fig.2c shows the results of FWENO schemes except FWENO15 and FWENO17. These two schemes obtain terrible results whose peak values for the Gaussian wave are 1.4 for FWENO15 and 19.2 for FWENO17. The remain results are worse than corresponding results of WENO-S schemes with the same order. Note that FWENO11 and FWENO13 behave worse than FWENO9 near  $x = 0.6$ .

Then, the end time  $t = 80$  and the number of mesh points  $N = 1000$  are employed. The results of WENO-S schemes are shown in Fig.3a. These results are very close to the exact solution. Fig.3b shows the results of WENO-M schemes and an enlarged view of the top right corner of the square wave is also given. It could be seen that oscillations happen for these schemes except WENO9-M. As for FWENO schemes, the results of three higher order ones are all NaN(not a number). And FWENO11 obtains a peak value about 2.7 in the square wave which is unacceptable. The remain one is the FWENO9 scheme, whose result is shown in Fig.3c. Compared with the result of WENO9-S scheme, the discontinuity profile of FWENO9 scheme for the square wave is wider and contains oscillations.

From the NaN appearing in the results, it could be inferred that solutions of the three highest order FWENO schemes blow up in the numerical simulation. So the results of an earlier time  $t = 2$  are considered. The peaks values are 1.68, 6.28 and 60.20 for FWENO13, FWENO15 and FWENO17 schemes respectively. The results of the other two are shown in Fig.4. FWENO9 obtains a good result, whereas FWENO11 scheme does not. From

Figure 2: Numerical results of advection of four kinds of waves, three kinds of WENO schemes,  $t = 8$  and  $N = 200$ .

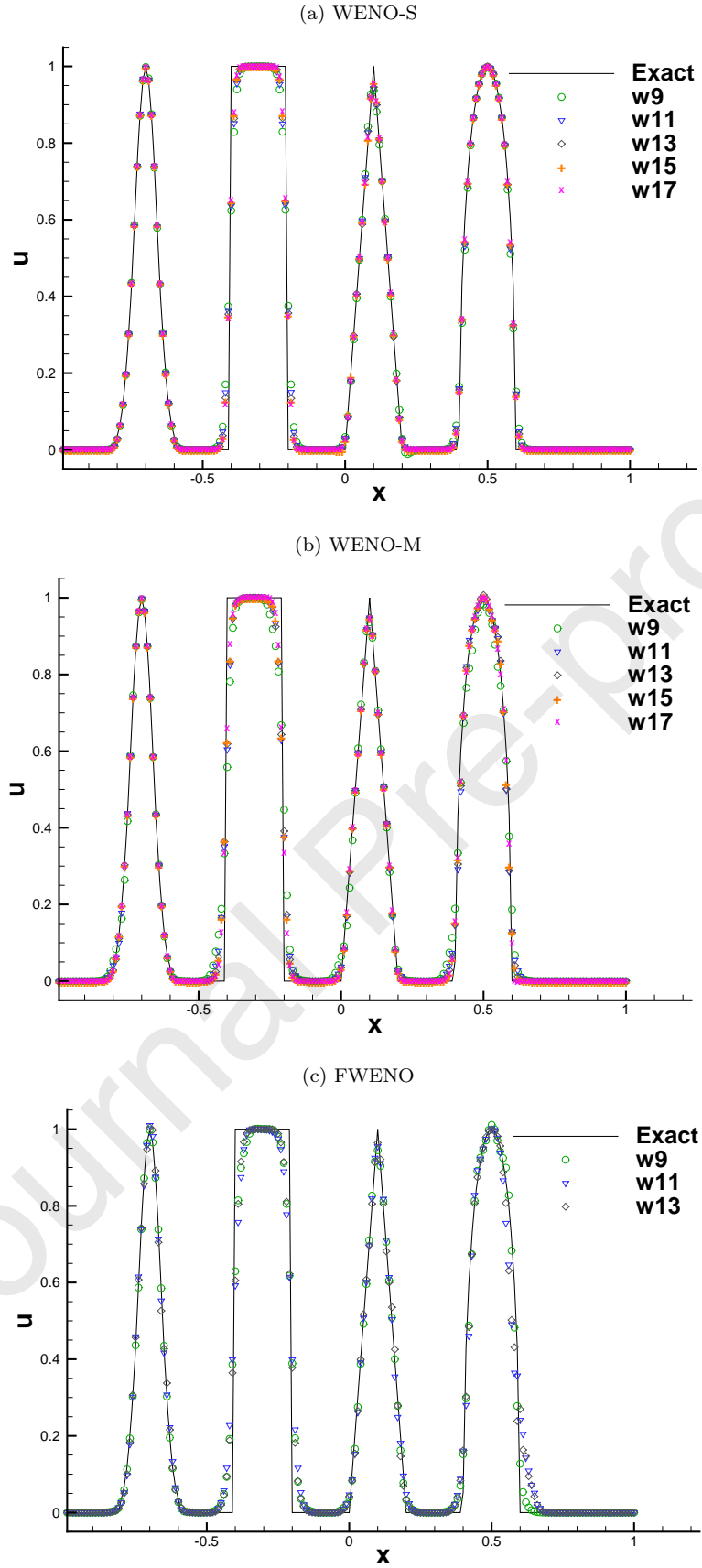


Figure 3: Numerical results of advection of four kinds of waves, three kinds of WENO schemes,  $t = 80$  and  $N = 1000$ .

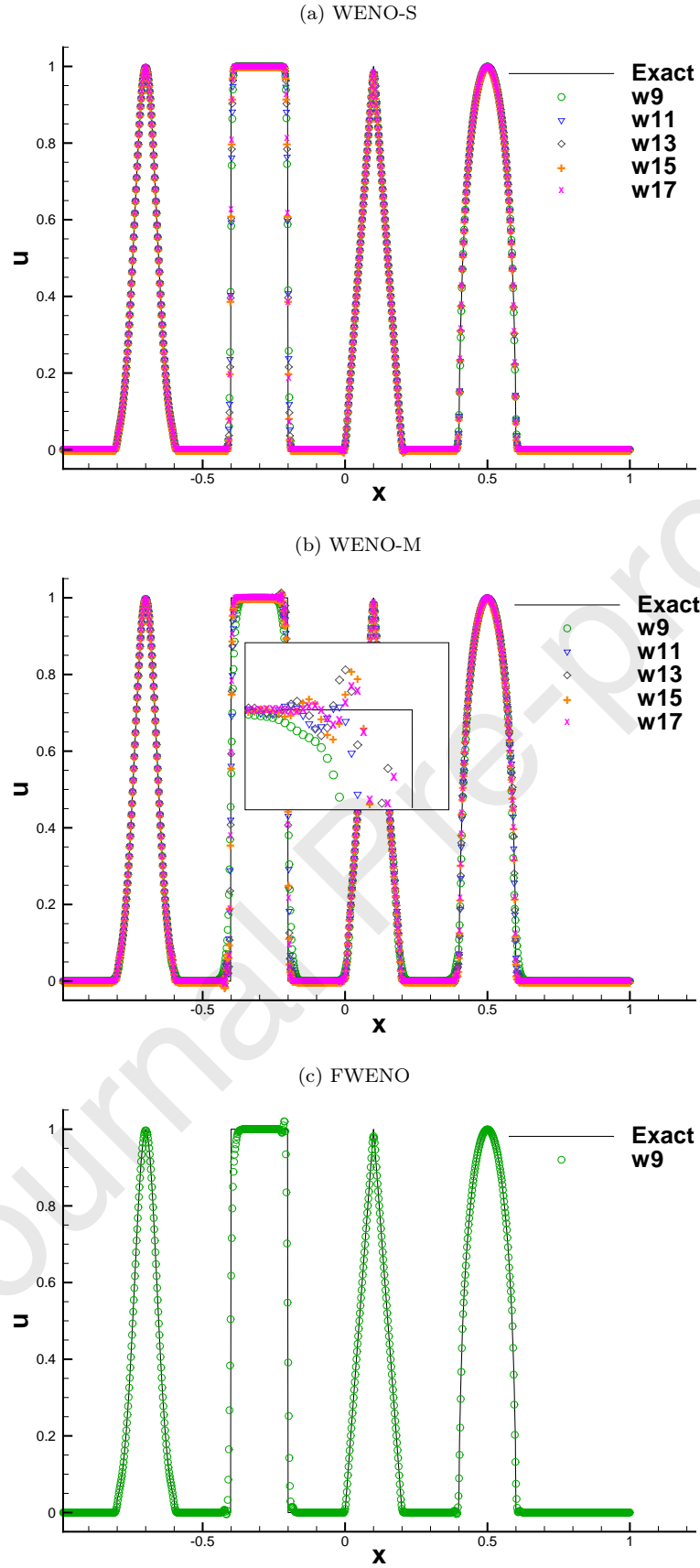
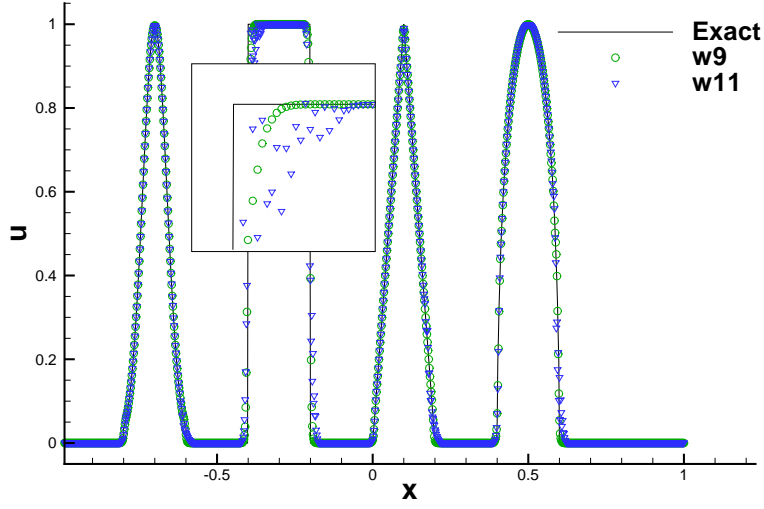


Figure 4: Numerical results of advection of four kinds of waves, FWENO9 and FWENO11 schemes,  $t = 2$  and  $N = 1000$ .



the enlarged view in the region  $x \in [-0.4, -0.35]$ , spurious oscillation which looks like a saw-tooth appears in the result of FWENO11. This will develop into more serious results, such as a peak value 2.7 at  $t = 8$  which has been stated above. Furthermore, FWENO9 scheme may also generate spurious result in some cases. For this problem, let's assume the end time  $t = 2000$ , the number of grids  $N = 400$ , and CFL number  $CFL = 0.1$ . The results of WENO9-S, WENO9-M and FWENO9 are shown in Fig.5. It can be observed that the result of FWENO9 scheme is unacceptable because of the large oscillations near  $x = -0.2$ . In the result of WENO9-M, the four kinds of waves become very smooth. In this test case, it is the WENO9-S scheme which obtains the best result.

On the whole, WENO-S schemes obtain the best results in these numerical tests. High order FWENO schemes are somewhat unreliable because the results can blow up for some cases. As for WENO-M schemes, they generate less accurate results than WENO-S schemes with the same order, and need more computational time.

(2) The second problem is the advection of a smooth sine wave modulated by a Gaussian centered at  $x = 1/2$ [38]. The governing equation is the same as before, but the initial profile is replaced with

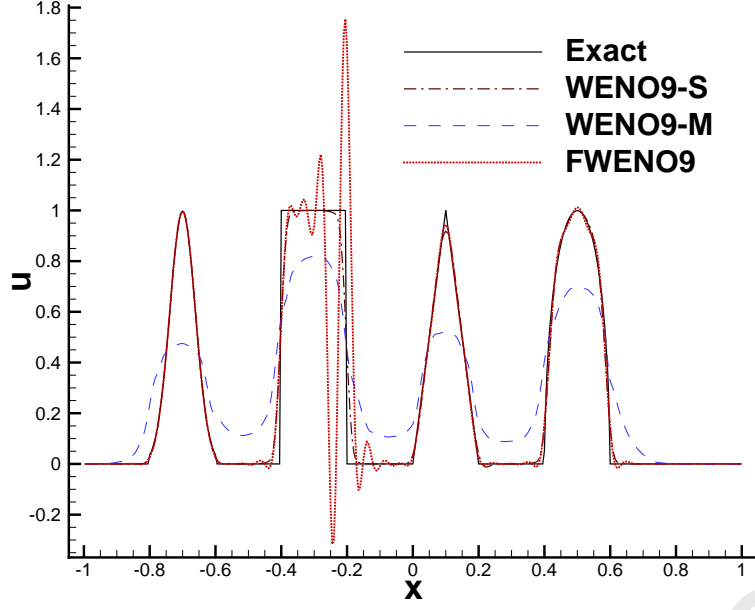
$$u_0(x) = \exp(-100(x - 1/2)^2) \sin(34\pi x). \quad (50)$$

The computational domain is  $x \in [0, 1]$  and the periodic boundary is implemented. The numerical solution over a mesh of 120 is advanced to  $t = 1$  with CFL number 0.5. The central parts of the results of WENO-S, WENO-M and FWENO schemes are shown in Fig. 6. It could be seen that the results of WENO-S schemes almost coincide with the exact solution except WENO9-S, which is also very close to it. The results of WENO-M schemes are slightly worse, and deviations from the exact solution could be viewed for the 9th order and the 11th order ones. As for FWENO schemes, the results are not so good except the 9th order one. The results of WENO11 show obvious oscillations in the right half of the wave packet. As the accuracy order of the scheme increases, the amplitude of oscillation becomes larger, and the region of oscillation becomes wider. For a better view, the results of FWENO15 and FWENO17 are not shown in this figure.

(3) The third problem under test is the linear propagation of sinusoidal disturbances in a medium with an abrupt change of the speed of sound[39, 40]. The governing equation is

$$\frac{\partial u}{\partial t} + c(x) \frac{\partial u}{\partial x} = 0. \quad (51)$$

Figure 5: The results of WENO9-S, WENO9-M and FWENO9 schemes for advection of four kinds of waves,  $t = 2000$ ,  $N = 400$  and  $CFL=0.1$ .



And the wave speed is piecewise constant given as

$$c(x) = \begin{cases} 2, & x \leq 0, \\ 1, & x > 0. \end{cases} \quad (52)$$

Computational domain is modified to  $[-2, 3]$  which is larger than the original problem and the inflow boundary is

$$u(-2, t) = 1 - 0.1 \sin(4\pi t). \quad (53)$$

According to Rankine-Hugoniot jump relations, the exact solution after  $t = 4$  is

$$u(x, t) = \begin{cases} 1 + 0.1 \sin(2\pi(x - 2t)), & x \leq 0, \\ 2 + 0.2 \sin(4\pi(x - t)), & x > 0. \end{cases} \quad (54)$$

The grid point number is set as 60 here. The points per wavelength (PPW) [41] of the profile are 12 and 6 for  $x \leq 0$  and  $x > 0$  respectively. The results at  $t = 8$  with CFL number 0.5 are given in Fig.7 where the enlarged views of the last wave crest are also shown. From these results, it could be found that WENO-S and FWENO schemes get better results. And WENO-M schemes obtain lower peak values.

(4) To evaluate the performance of WENO schemes near high order critical points, the second problem in accuracy order tests will be considered again. That is advection of initial profile  $u(x, 0) = \sin^4(\pi x)$  with the end time  $t = 2$ . Here the numerical errors of some WENO schemes with the same order will be compared and shown in Fig 8. To save space, only the 9th, 13th and 17th order schemes are considered. From the figures, it could be observed that WENO-S and FWENO schemes behave better than WENO-M schemes.

(5) Another problem in accuracy order tests is also considered again. The governing equation is inviscid Burgers equation and the initial profile is  $u(x, 0) = 0.5 + \sin(\pi x)$  with  $x \in [-1, 1]$ . The periodic boundary is implemented and the grid number is set as  $N = 80$ . However the end time is set as  $t = 71$  and a shock exists in the entropy solution. In fact it has moved a distance of  $71/2 - 1/(2\pi)$  after its generation. The numerical results are given in Fig 9, and all schemes can capture this shock well. After careful observation, WENO-S could obtain slightly better results than FWENO which in turn behaves better than WENO-M.



Figure 6: Numerical results of WENO-S, WENO-M and FWENO schemes for advection of modulated sine wave,  $t = 1$  and  $N = 120$ .

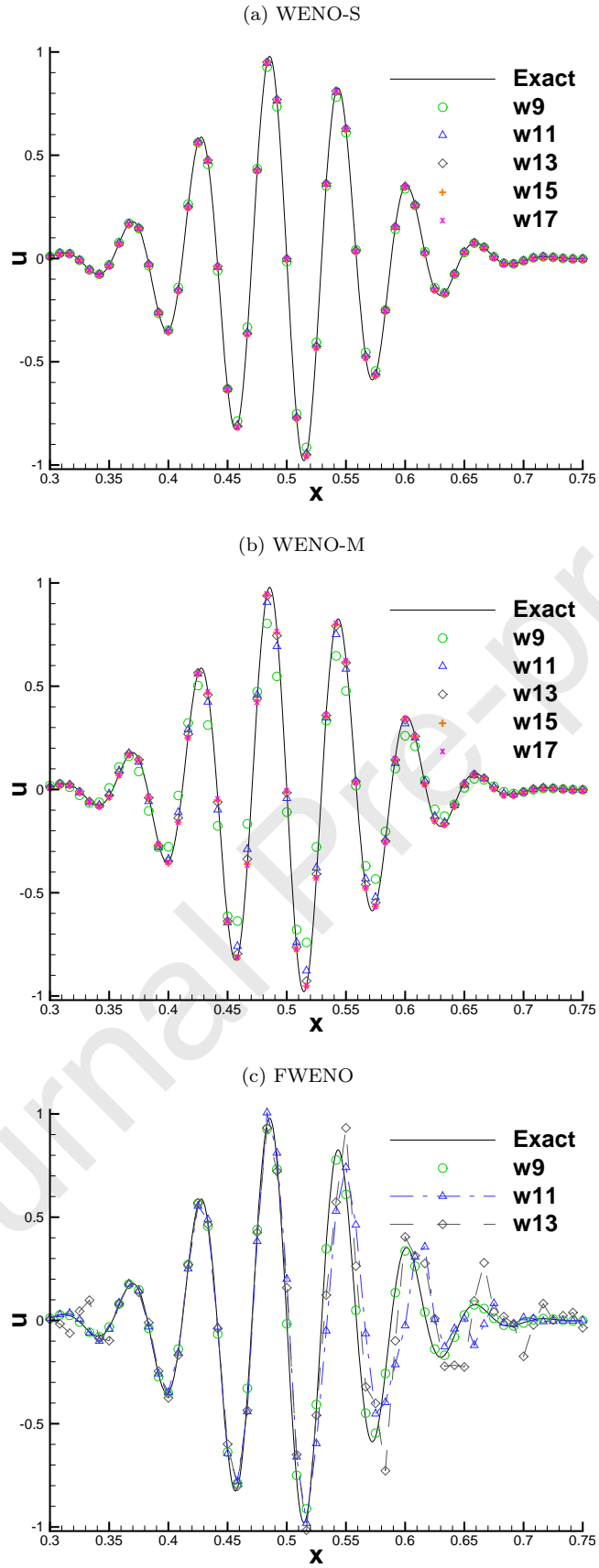


Figure 7: Numerical results of WENO-S, WENO-M and FWENO schemes for a sound wave refraction problem for  $t = 8$  and  $N = 60$ . Enlarged view of the last wave crest are shown in the lower right corner.

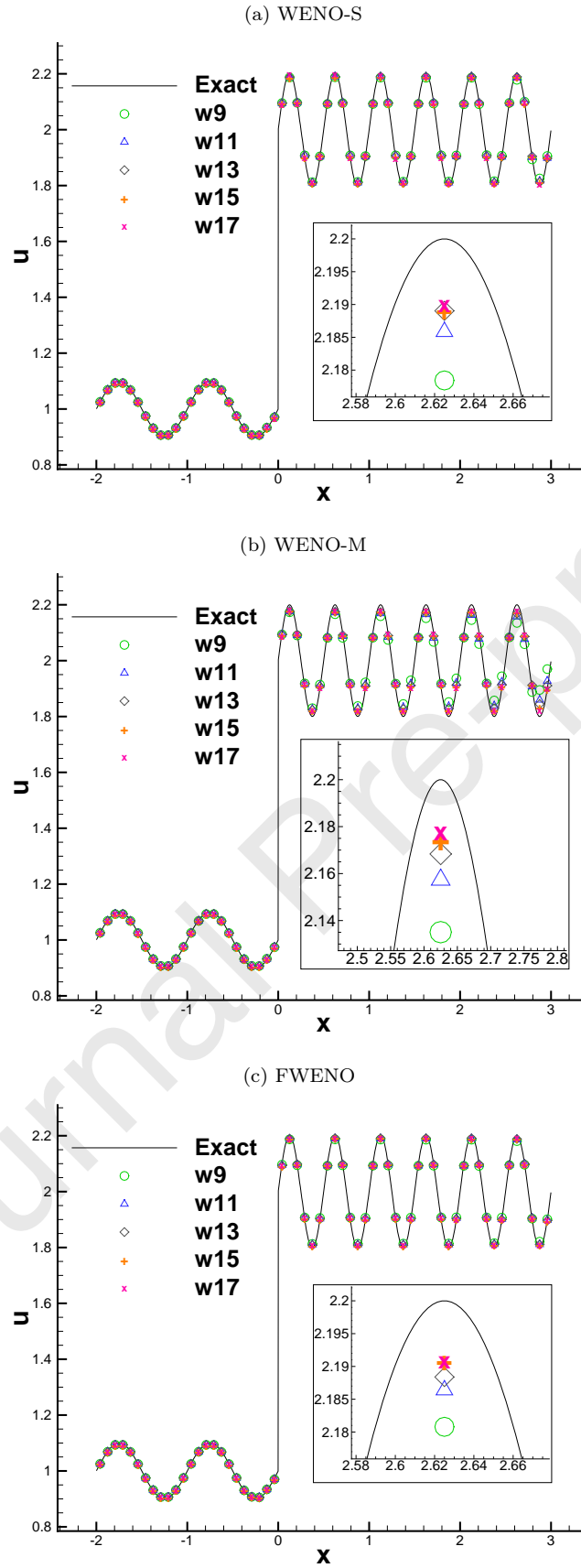


Figure 8:  $L_1$  and  $L_\infty$  errors of numerical results for advection of  $\sin^4(\pi x)$  with grid points  $N = 20, 40, 80, 160$ . Schemes: WENO-S, WENO-M and FWENO schemes of 9th, 13th and 17th order.

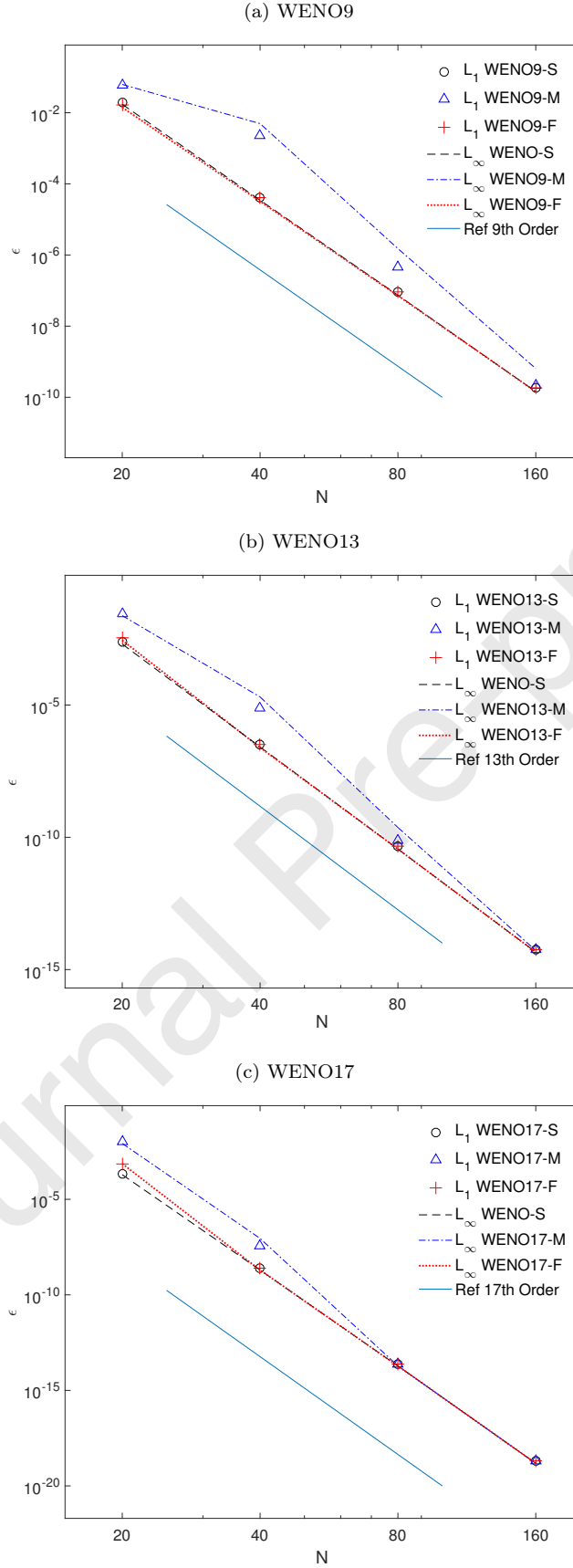
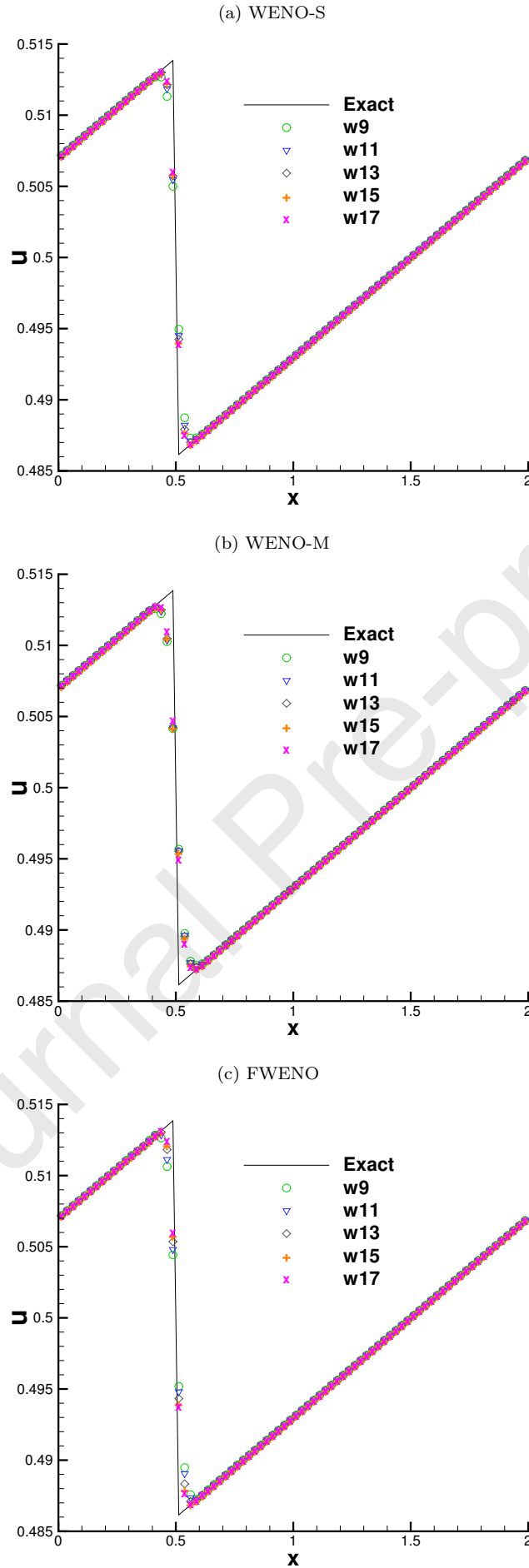


Figure 9: Numerical results of WENO-S, WENO-M and FWENO schemes for Burgers equation with problem for  $t = 71$  and  $N = 80$ .



## 7 The case of Euler equations

In this section, the new WENO schemes will be used to solve Euler equations. In these computations, the techniques of local Lax-Friedrichs splitting and the local characteristic-wise projection are employed[8]. We refer to [6] for more details. For very high order WENO schemes, another technique which should be implemented is the order reduction procedure near discontinuities[8]. In this section, the order reduction procedure will be introduced firstly. Then the numerical simulations for 1D problems and 2D problems will be carried out in order. If not specified, the third order Runge-Kutta method is employed as the time integration approach, and CFL number is set as 0.25 for numerical tests in this section, with which there is no apparent overshooting or undershooting in the numerical results of advection of square waves.

### 7.1 Predetermined order reduction methodology

The stability properties of very high order WENO schemes are worse than those of low order ones. One reason is that the small dissipation of the high order schemes could not suppress the oscillations effectively. The second should be attributed to their wide stencils which could contain more than one discontinuity. Then the functions on all sub-stencils are discontinuous and the weighted procedure cannot lead to an essentially non-oscillatory result. The third is the Runge phenomenon for high order interpolation or reconstruction. The numerical fluxes obtained from off-centered wide sub-stencils may lead to large errors which could also affect the stability. As for Euler equations, the situation is even worse for very high order WENO schemes because of the interaction between different characteristic fields. Serious oscillations may appear in the numerical results of these high order schemes, and the computations are more likely to be broken. In [8], a recursive order-reduction (ROR) procedure was proposed to deal with this problem. This method needs the reconstruction value of  $\rho$  and  $p$  at the cell interface. However, for the methodology of the present work, the reconstruction is taken on the flux. Thus, this ROR procedure could not be implemented directly in the present work and another method will be developed.

A predetermined order reduction method is considered here. The aim of the order reduction is to overcome the problems caused by the numerical simulation of interactions between discontinuities of different characteristic fields. For most of the interactions there are one or more nonlinear fields involved in. As for comparatively rare interactions between linear fields, they will hardly cause big problems unless large variations in some nonlinear fields are generated. But these variations, to some degree, can be considered as discontinuities. So, nonlinear discontinuities could be treated as the object to trigger the order reduction. Thus, this reduction will not work for most linear discontinuities, and this will be helpful to obtain sharp profiles for contact discontinuities. Note that it is more difficult to keep sharp profile for contact discontinuities compared with nonlinear ones. For Euler equations, the pressure could be used to distinguish the nonlinear discontinuities from linear discontinuities. So it will be used to judge whether order reduction is needed or not. Here the criterion of employing WENO(2m-1)-S for the numerical flux is proposed as that the smoothness indicators of the pressure satisfy

$$\beta^{2m(S)} \leq 4\beta^{2m-2(S)}. \quad (55)$$

The stencils used for these two smoothness indicators have the same midpoint where the numerical flux is computed. If this inequality is not satisfied, the WENO(2m-3)-S scheme will be taken into consideration. Then this procedure will be repeated, and  $m$  in the inequality is replaced with  $m - 1$ . This recursive procedure will go on until the inequality stands or  $m$  reaches 3. As  $m$  equates to 3, WENO5-M is employed because WENO(2r-1)-S schemes are only available for  $r \geq 4$ .

Let's examine the inequality (55). It could be found from Table 4 that the coefficients of three terms in  $\beta^{(S)}$  increases rapidly as the stencil becomes wider. Thus,  $\beta^{(S)}$  will increase greatly for discontinuous profile with the broadening of the stencil. As for the multiplier 4 in the right hand side, it is under the assumption that  $\delta^2\phi f$  could be comparable to  $2\phi f$  when  $f$  is neither very smooth nor discontinuous. Here  $\delta^2\phi f$  and  $\phi f$  represent the three terms  $a, b, c$  in  $\beta^{2m(S)}$  and  $\beta^{2m-2(S)}$  respectively. After calculation, we found that this inequality does not hold true for step function if the discontinuity is in the stencil. Furthermore, it can hardly be satisfied if the profile is discontinuous on the  $2m$ -point stencil. Therefore, with this criterion, employing very high order schemes is probably avoided near the nonlinear discontinuities. For the case that the pressure is very smooth in this region, the left hand side and right hand side of inequality (55) will be  $O(h^{4m-4})$  and  $O(h^{4m-8})$  respectively. So, this inequality will hold true and the WENO(2m-1)-S scheme is employed.

A specific case can be discussed is that the function of pressure is a monochromatic wave  $f(x) = A \sin(kx + B) + C$ , where  $A, B, C$  and  $k$  are constants. Then the inequality will be

$$2^{4m-2} A^2 \sin^{4m-4}(kh/2) \cos^2(kh/2) \leq 4 \cdot 2^{4m-6} A^2 \sin^{4m-8}(kh/2) \cos^2(kh/2).$$

For  $kh \in (0, \pi)$ , it will lead to

$$kh \leq \pi/2.$$

This corresponds to PPW no less than 4. Then, for monochromatic pressure waves with  $PPW \geq 4$ , the inequality holds true and order reduction do not occur for the proposed WENO schemes. However, for monochromatic pressure waves with  $PPW < 4$ , the inequality is never satisfied in the order reduction procedure, and finally the method will be reduced to the WENO5-M scheme. In fact, these kinds of waves could be non-physical oscillations which should be prevented. Therefore, a relatively dissipative scheme should be employed to damp them. WENO5-M scheme is more dissipative than WENO(2m-1)-S for  $m \geq 4$ , and hence it is appropriate to apply this scheme for waves with  $PPW < 4$ .

In the numerical simulations of Euler equations using high order schemes, negative pressure is more likely to appear in the simulation of very strong shocks which will break the computation. Negative pressure arises when the computed kinetic energy exceeds the total energy [42]. To avoid this, another criterion of order reduction will be considered. For 1D inviscid flow, the governing equation of pressure is

$$p_t + \gamma p u_x + u p_x = 0.$$

In this equation  $\rho, u, \gamma$  represent the density, velocity and the ratio of specific heats respectively. We require that the variation of pressure in a time step should be less than its value. Therefore the criterion for numerical flux at point  $x_{i_0} + h/2$  is proposed as

$$\gamma \max_j p_j \cdot \left( \max_i |u_{i+1} - u_i| \right) + \max_j |u_j| \cdot \left( \max_i |p_{i+1} - p_i| \right) \leq \frac{1}{d} \cdot \frac{h}{\Delta t} \min_j p_j, \quad (56)$$

$$i \in \{i_0 - m + 1, \dots, i_0 + m - 1\}, j \in \{i_0 - m + 1, \dots, i_0 + m - 2\},$$

where  $h$  and  $\Delta t$  are the mesh size in the current direction and the time step respectively. With the consideration of multi-dimensional case, parameter  $d$  appears in this inequality which represents the number of the spatial dimensions.

The order reduction procedure is described with pseudo code for computing a numerical flux as follows.

```

m = r;
do while m > 3
    if both Eq.(55) for pressure and Eq.(56) are true
        exit loop;
    else
        m = m - 1;
    end if
end do
if m > 3

    run WENO(2m-1)-S with LLF splitting and local characteristic decomposition.
else

    run WENO(2m-1)-M with LLF splitting and local characteristic decomposition.
end if

```

This procedure should be more efficient than the ROR procedure in [8], since the WENO scheme employed is predetermined. The WENO-S schemes with this predetermined order reduction method are called as PORWENO-S schemes in this paper. They are robust which will be shown in the numerical tests. However, the WENO5-M scheme could fail in some extreme tough problems, which will also be a trouble for the proposed methods. For these extreme problems, a further order reduction is needed to obtain reasonable numerical results. Then the WENO3-M or even the first order upwind scheme should be employed. However, it is not considered in the present work, since the proposed methods achieve stable results for all test cases in the numerical simulations.

## 7.2 Numerical tests for 1D Euler equations

The governing equations of one-dimensional inviscid flow are

$$U_t + F(U)_x = 0, \quad (57)$$

with

$$U = (\rho, \rho u, E)^T, \quad F(U) = (\rho u, \rho u^2 + p, u(E + p))^T. \quad (58)$$

The equation of the state is

$$p = (\gamma - 1) \left( E - \frac{1}{2} \rho u^2 \right), \quad (59)$$

where  $\rho, u, p, E$  and  $\gamma = 1.4$  are density, velocity, pressure, total energy and the ratio of specific heats respectively. In this subsection and the next subsection, the PORWENO(2r-1)-S schemes are employed to simulate some inviscid flow problems. The results of WENO5-M for some test cases are also given to illustrate the effect of the order reduction procedure.

(1) The proposed order reduction method will not degrade the accuracy order for smooth profile. As the grid length is very small, Eq.(55) for pressure will hold true since  $O(h^{4m-4})$  is less than  $O(h^{4m-8})$ . As for Eq. (56), the differences of  $p$  and  $u$  will also be very small true when  $h$  is a tiny value. Thus, this inequality will be true since  $h/\Delta t$  is required to be greater than some value which is determined by the CFL condition.

The 1D Euler equation with a source term is taken into consideration. The exact solution is set as

$$(\rho, u, p) = \left( 1, 0, 1 + 0.5 \sin \left( \pi(x - t) - \frac{\sin(\pi(x - t))}{\pi} \right) \right)^T, \quad (60)$$

and the modified 1D Euler equations will be

$$U_t + F(U)_x = S, \quad (61)$$

where  $U$  and  $F$  have the same meanings as those in Eq. (58). The source term is

$$S = (0, a, -a/(\gamma - 1))^T, \quad a = 0.5 \cos \left( \pi(x - t) - \frac{\sin(\pi(x - t))}{\pi} \right) (\pi - \cos(\pi(x - t))). \quad (62)$$

Although there is an additional source term, we do not modify the criterion Eq.(56) in this test case. The program adopts the 128-bit floating point calculation such that round-off errors has almost no effect on the results. Since the governing equations are nonlinear, the fourth order Runge-Kutta method is employed like the accuracy test example for Burgers equation. Also as the grid length is halved the time step will be multiplied by  $2^{-(2r-1)/4}$  for PORWENO(2r-1)-S scheme. The results are shown in Table 14. From this table, it could be observed that the desired accuracy orders of  $L_1$  errors have been achieved. However the  $L_\infty$  orders are slightly smaller than the anticipated values, and this is going better when finer grid is employed.

(2) Two shock tube problems are tested here. The first is the Lax problem which is initiated as

$$(\rho, u, p) = \begin{cases} (0.445, 0.698, 3.528), & x \in [-0.5, 0), \\ (0.500, 0.000, 0.571), & x \in [0, 0.5], \end{cases} \quad (63)$$

and the end time is  $t = 0.16$ . The second is the Sod problem initiated as

$$(\rho, u, p) = \begin{cases} (1.000, 0.750, 1.000), & x \in [-0.5, 0), \\ (0.125, 0.000, 0.100), & x \in [0, 0.5], \end{cases} \quad (64)$$

with end time  $t = 0.2$ .

Three sets of grids with grid numbers  $N = 100, 200, 400$  are considered. The density profiles of the results are shown in Fig.10 and Fig.11. From the figures, it could be seen that all schemes have similar behaviors. That means the order reduction procedure works, and the proposed PORWENO(2r-1)-S schemes are reduced to WENO5-M at those nonlinear discontinuities. However, near contact discontinuities, it seems that they do not outperform WENO5-M. This could be attributed to two reasons. At first, the numerical results could be greatly affected by those several initial steps for Riemann problems[43]. For these steps, the proposed schemes are reduced to WENO5-M scheme at contact discontinuities, since they are very close to the shocks. The other should be that the simulation time may not be so long to show their differences.

(3) The shock-entropy wave problem is considered here whose initial condition is [6]

$$(\rho, u, p) = \begin{cases} (3.857143, 2.629369, 31/3), & x \in [-5, -4), \\ (1 + 0.2 \sin(kx), 0, 1), & x \in [-4, 5]. \end{cases} \quad (65)$$

Table 14: Convergence orders of the new  $(2r - 1)$ -point WENO schemes for modified 1D Euler equations.

N	$L_1$ error	$L_1$ order	$L_\infty$ error	$L_\infty$ order
$r = 5$				
20	1.967E-04		3.730E-04	
40	3.694E-07	9.057	1.289E-06	8.176
80	7.663E-10	8.913	4.913E-09	8.036
160	1.453E-12	9.043	1.250E-11	8.619
$r = 6$				
20	1.672E-04		3.800E-04	
40	9.579E-08	10.769	3.336E-07	10.154
80	4.813E-11	10.959	3.176E-10	10.037
160	2.291E-14	11.037	1.943E-13	10.675
$r = 7$				
20	1.675E-04		3.805E-04	
40	2.427E-08	12.752	9.053E-08	12.037
80	3.013E-12	12.976	2.035E-11	12.119
160	3.589E-16	13.036	3.041E-15	12.709
$r = 8$				
20	1.675E-04		3.808E-04	
40	6.001E-09	14.768	2.322E-08	14.001
80	1.897E-13	14.949	1.295E-12	14.130
160	5.612E-18	15.045	4.762E-17	14.731
$r = 9$				
20	1.674E-04		3.808E-04	
40	1.514E-09	16.755	5.947E-09	15.967
80	1.189E-14	16.957	8.198E-14	16.146
160	8.773E-20	17.049	7.454E-19	16.747

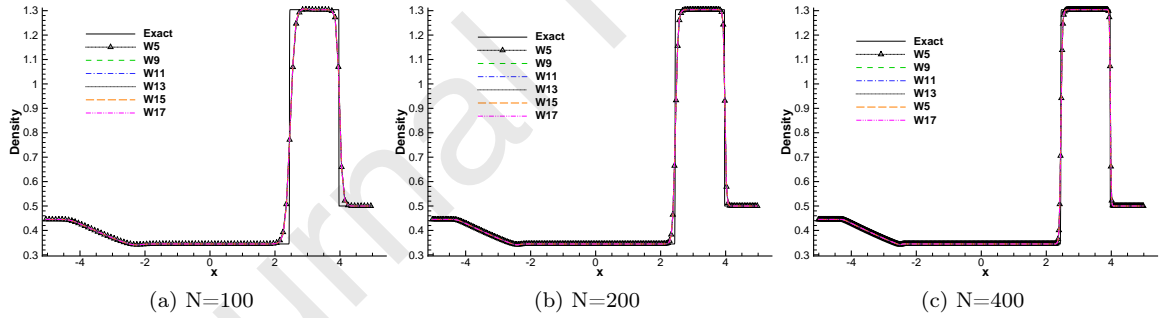
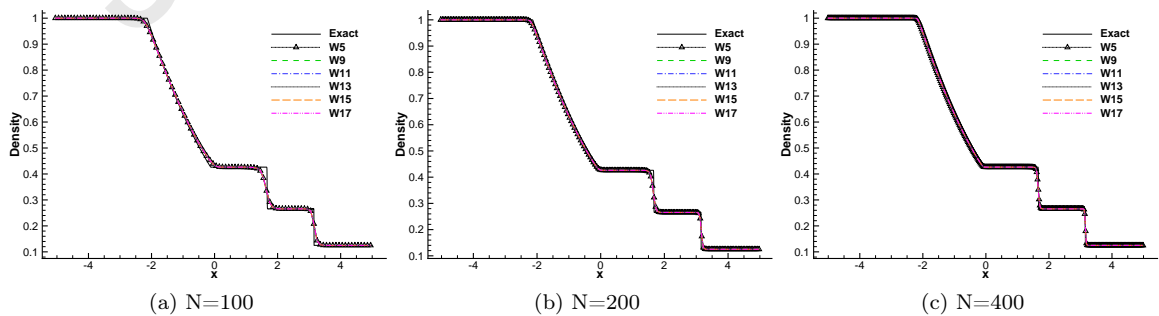
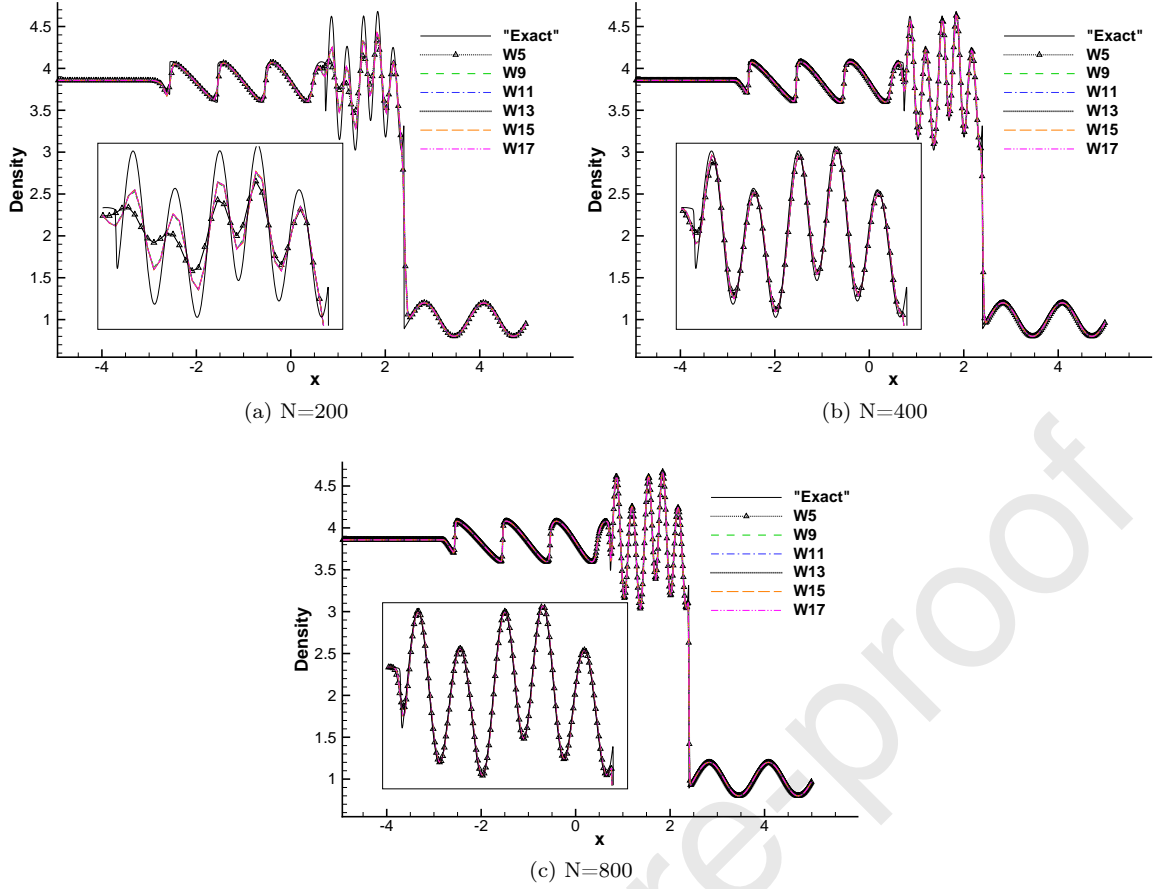
Figure 10: Density profiles of numerical results at  $t = 0.16$  for Lax problem, W5 represents WENO5-M scheme and  $W_\alpha$  represents PORWENO $\alpha$ -S for  $\alpha \geq 9$ .Figure 11: Density profiles of numerical results at  $t = 0.2$  for Sod problem. W5 represents WENO5-M scheme and  $W_\alpha$  represents PORWENO $\alpha$ -S for  $\alpha \geq 9$ .



Figure 12: Density profiles of numerical results at  $t = 1.8$  for shock-entropy wave problem. W5 represents WENO5-M scheme and  $W\alpha$  represents PORWENO $\alpha$ -S for  $\alpha \geq 9$ .



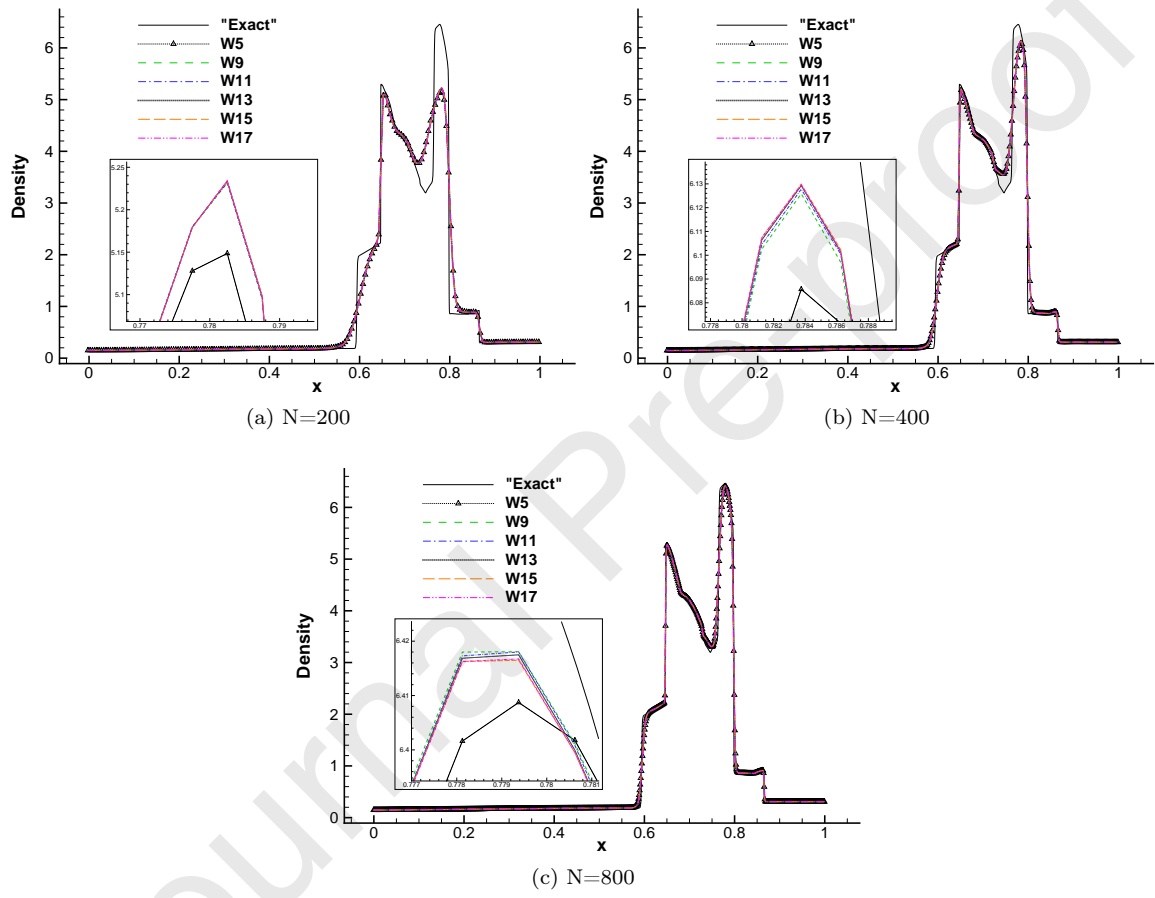
with wavenumber  $k = 5$ . In this problem, a right-moving (Mach 3) shock wave interacts with a density disturbance that generates a flow field with both smooth structures and discontinuities. The density profiles of the numerical results at  $t = 1.8$  with grid numbers  $N = 200, 400, 800$  are shown in Fig.12. The “Exact” value in the figures represents the result obtained by fifth order WENO-JS scheme with 4000 grid points. For  $N = 200$ , all these methods cannot obtain accurate results near the high-wavenumber wave region. There are no visible differences among the results of the PORWENO(2r-1)-S schemes which could be separated only by further enlarging this area. These results are much better than those of WENO5-M, which demonstrates the advantage of high order WENO-S schemes. As the grid number increases, the numerical results are more close to the “Exact” value. And the most obvious differences are located in the two ends of this high-wavenumber wave region, where the result of WENO5-M could be separated more easily from the results of proposed methods. Note that the results of the proposed method are much better than those of RORWENO with the same order, which were shown in Fig.10 of Ref [8].

(4) The interaction of two blast waves is taken into consideration[44]. The initial condition is

$$(\rho, u, p) = \begin{cases} (1, 0, 1000), & x \in [0, 0.1), \\ (1, 0, 0.01), & x \in [0.1, 0.9), \\ (1, 0, 100), & x \in [0.9, 1]. \end{cases} \quad (66)$$

The end time is  $t = 0.038$  and the reflecting boundary condition is applied in both sides. The density of the numerical results on grids with  $N = 200, 400, 800$  are shown in Fig.13. In these figures, the “Exact” value represents the result obtained by fifth order WENO-JS scheme with 8000 grid points. Although the differences of the numerical results are small, it could be viewed in the enlarged figures near  $x = 0.78$ . From these enlarged views, it could be observed that the proposed PORWENO(2r-1)-S schemes obtain larger peak values than those of WENO5-M. Also, the proposed method behaves better than RORWENO schemes for this problem whose results were shown in Fig.14 of Ref[8].

Figure 13: Density profiles of numerical results at  $t = 0.038$  for the interaction of two blast waves problem. W5 represents WENO5-M scheme and  $W\alpha$  represents PORWENO $\alpha$ -S for  $\alpha \geq 9$ .



### 7.3 Two-dimensional problems

In this subsection, the two-dimensional inviscid flow is taken into consideration, whose governing equations can be written as

$$U_t + F(U)_x + G(U)_y = S, \quad (67)$$

with

$$U = (\rho, \rho u, \rho v, E)^T, \quad F(U) = (\rho u, \rho u^2 + p, \rho uv, u(E + p))^T, \quad G(U) = (\rho v, \rho uv, \rho v^2 + p, v(E + p))^T. \quad (68)$$

$S$  is the source term. The equation of the state is

$$p = (\gamma - 1) \left( E - \frac{1}{2} \rho u^2 \right), \quad (69)$$

where  $\rho, u, v, p, E$  and  $\gamma$  are density, velocity in  $x$  direction, velocity in  $y$  direction, pressure, total energy and the ratio of specific heats respectively. For the first four test cases,  $\gamma$  is set as 1.4 and there is no source term. The remain test case is the Rayleigh-Taylor instability problem, where  $\gamma = 5/3$  is employed and  $S = [0, 0, \rho, \rho v]^T$ . According to the results of 1D problems in the last subsection, PORWENO(2r-1)-S for  $r \geq 5$  have similar behaviors for inviscid problem with discontinuities. Thus, some numerical results are omitted to save space.

(1) The effect of proposed order reduction method in smooth region will be considered first. The advection of a smooth compressible vortex[7, 8] is employed as the test case. In this problem, an isentropic vortex is added to a mean flow of  $\rho = 1, p = 1$  and  $(u, v) = (1, 1)$ . The temperature is  $T = p/\rho$  and the entropy is  $S = p/\rho^\gamma$ . The perturbation values caused by the vortex are

$$(\delta u, \delta v) = \frac{\epsilon}{2\pi} e^{\frac{1-r^2}{2}} (-\bar{y}, \bar{x}), \quad \delta T = -\frac{(\gamma-1)\epsilon^2}{8\gamma\pi^2} e^{1-r^2}, \quad \delta S = 0,$$

where  $(\bar{x}, \bar{y}) = (x - 5, y - 5), r^2 = \bar{x}^2 + \bar{y}^2$ , and the vortex strength  $\epsilon = 5$ . Periodic boundary treatment is implemented in both two directions which could be considered as a good approximation to infinite array of vortices. Note that the velocity field of this vortex is not periodic[8] and small errors will be generated because this boundary treatment.

The numerical schemes used are WENO(2r-1)-S schemes for  $5 \leq r \leq 9$  with and without implementation of the proposed order reduction method. The  $L_1$  and  $L_\infty$  errors on four sets of grids  $20 \times 20, 40 \times 40, 80 \times 80$  and  $160 \times 160$  are given in Fig. 14. From these figures, it could be observed that the errors will become larger or smaller with the employment of this order reduction method. However, two relatively obvious patterns could be found. One is that when coarser grids together with relatively higher order schemes or finer grids with relatively lower order schemes are adopted, this method will play a negative role. Another is this method will lead to smaller  $L_1$  errors at grid  $80 \times 80$ . Roughly speaking, the impact of this order reduction method on the accuracy of the WENO schemes is not very clear, and it is not great which could be observed from the figures.

(2) The fifth 2D Riemann problem proposed in [45] is taken into consideration. The computational domain is  $[0, 1] \times [0, 1]$ , and the initial state is given by

$$(\rho, u, v, p) = \begin{cases} (1, -0.75, -0.5, 1), & x \geq 0.5, y \geq 0.5, \\ (2, -0.75, 0.5, 1), & x < 0.5, y \geq 0.5, \\ (3, 0.75, -0.5, 1), & x \geq 0.5, y < 0.5, \\ (1, 0.75, 0.5, 1), & x < 0.5, y < 0.5. \end{cases} \quad (70)$$

The end time is 0.23. Three sets of grids  $N_x \times N_y = 200 \times 200, 400 \times 400, 800 \times 800$  are considered. The main structure of this problem only includes contact discontinuities and waves created by their interactions. The density contours of the numerical results are shown in Fig.15. It could be observed from this figure that more rollups of the slip line and more vortices could be observed with the increase of grid points. However, it seems that the difference among these three schemes are very small. In fact, PORWENO9-S and PORWENO17-S obtain slightly better results. At the coarsest grid  $N_x = N_y = 200$ , the rollup of the slip lines are better resolved by these two schemes. As for the other two grids, the differences could be observed after further enlarging the rollup of the slip lines.

Figure 14:  $L_1$  and  $L_\infty$  errors of vortex advection problem using different WENO schemes. Grids:  $20 \times 20$ ,  $40 \times 40$ ,  $80 \times 80$  and  $160 \times 160$ .

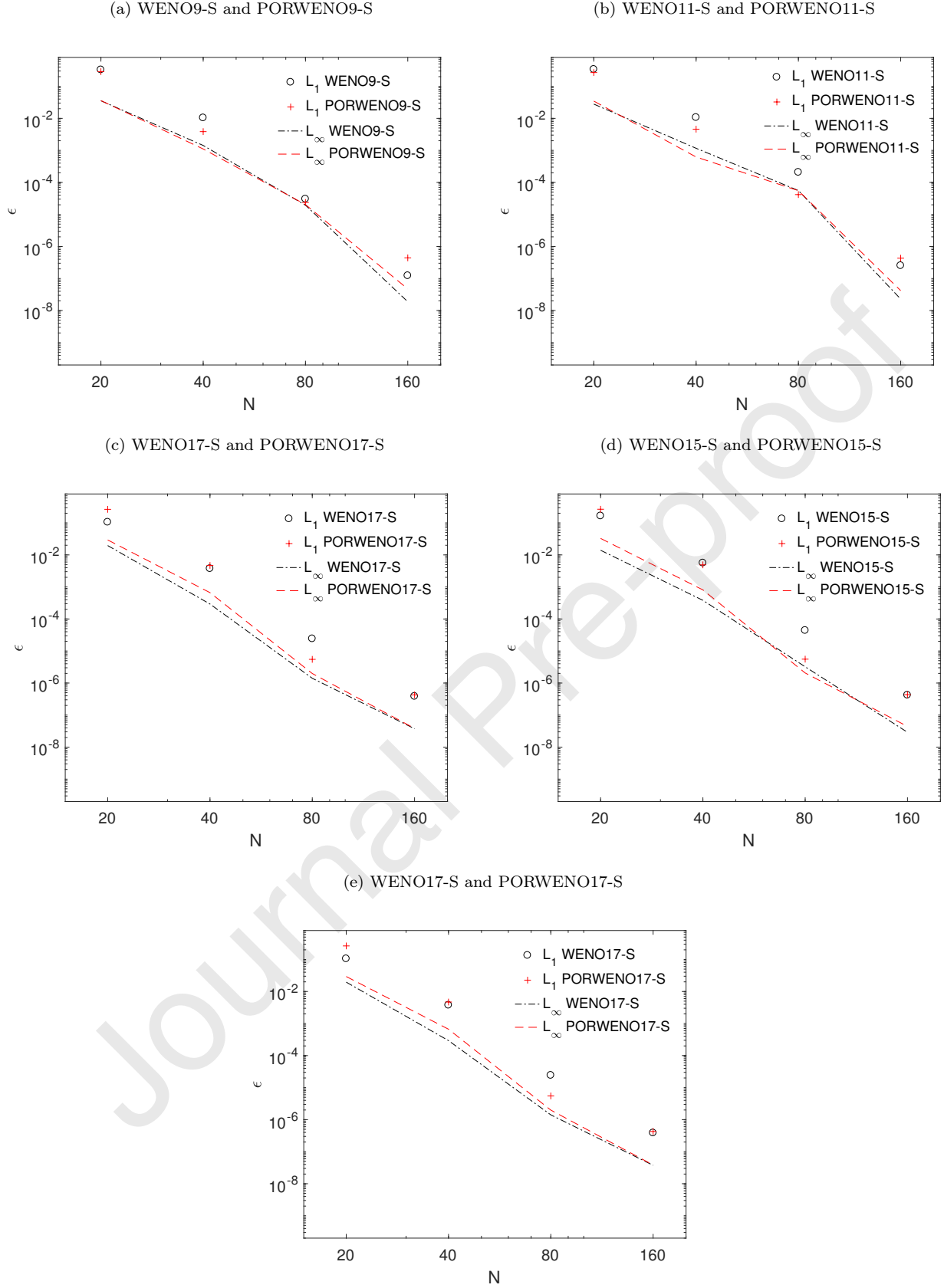
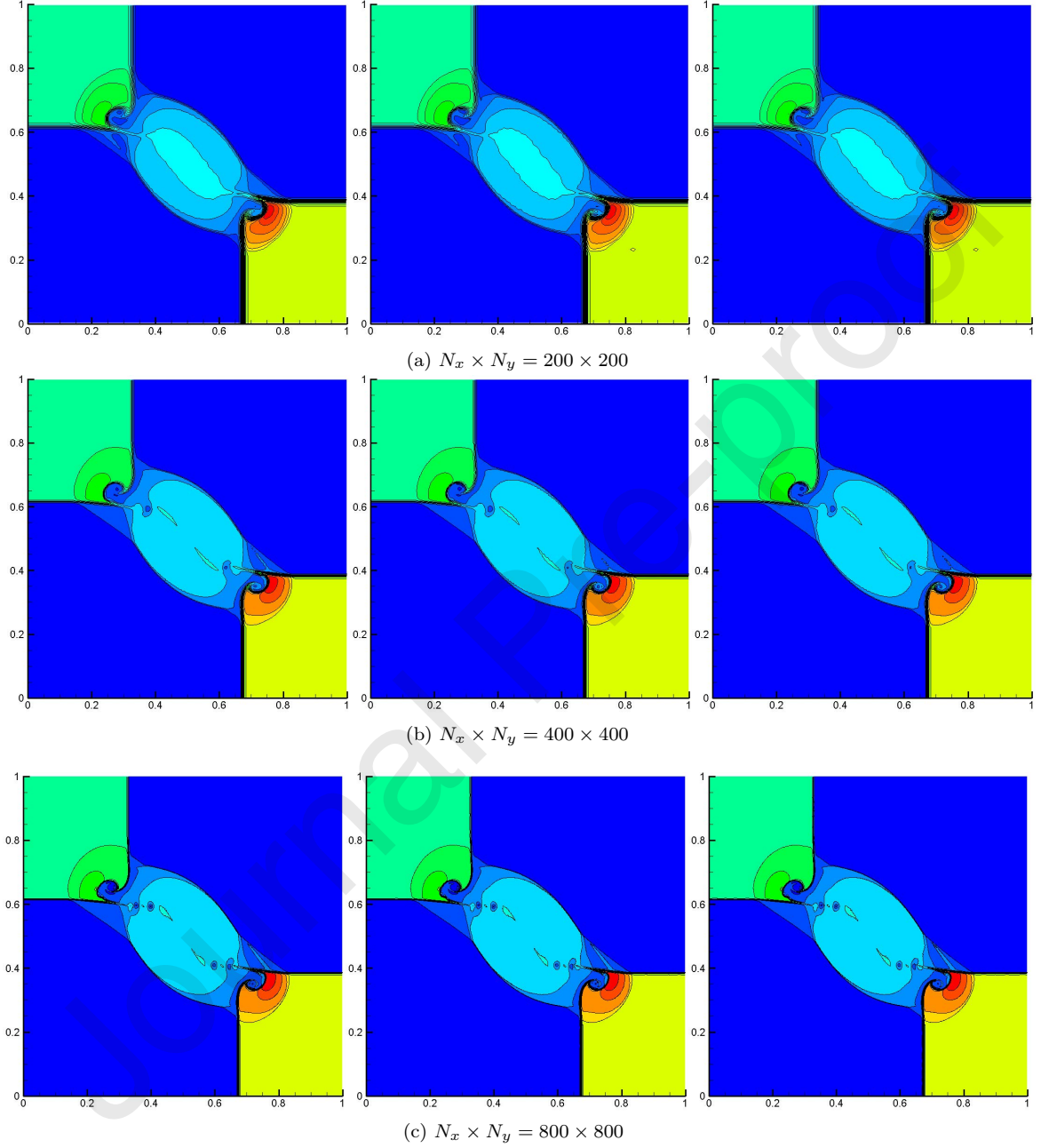


Figure 15: Numerical results at  $t = 0.23$  of three different schemes for the fifth 2D Riemann problem in [45], density contours. From left to right: WENO5-M, PORWENO9-S and PORWENO17-S.



(3) Another 2D Riemann problem proposed in [46, 45] is taken as the test case. The computational domain is also  $[0, 1] \times [0, 1]$ , whereas the initial state is

$$(\rho, u, v, p) = \begin{cases} (1.5, 0, 0, 1.5), & x \geq 0.8, y \geq 0.8, \\ (0.5323, 1.206, 0, 0.3), & x < 0.8, y \geq 0.8, \\ (0.5323, 0, 1.206, 0.3), & x \geq 0.8, y < 0.8, \\ (0.138, 1.206, 1.206, 0.029), & x < 0.8, y < 0.8. \end{cases} \quad (71)$$

The end time is set as 0.8. Three sets of grids are also set as  $N_x \times N_y = 200 \times 200, 400 \times 400, 800 \times 800$ . In Fig.15 the density contours of the numerical results are given. As the grids are refined, more structures can be resolved by the numerical schemes. For this problem, PORWENO9-S and PORWENO17-S can resolve much more small structures than WENO5-M. The differences between the results of PORWENO17-S and PORWENO9-S are also very small except those of grid  $800 \times 800$ . For this finer grid, there are more rollups in the stem pointing northeast in the result of PORWENO17-S.

(4) The double Mach reflection problem is considered[44]. In this problem, a right moving Mach 10 shock forms  $60^\circ$  angle with a flat plate. The initial position of the shock is  $(x, y) = (1/6, 0)$  which is the head of the plate. At the beginning, two states of flow are separated by this shock. The undisturbed stationary state has density  $\rho = 1.4$  and pressure  $p = 1$ . The exact post-shock condition is imposed for the left boundary and the region  $x \leq 1/6$  on the bottom boundary. For  $x > 1/6$  on the bottom, the reflecting boundary is implemented. At the top, the boundary is set to follow the moving oblique shock. Outflow boundary condition is imposed on the right boundary. The computational domain of the problem is  $[0, 4] \times [0, 1]$ , and the end time of simulation is  $t = 0.2$ . Three grids  $N_x \times N_y = 400 \times 100, 800 \times 200$  and  $1600 \times 400$  are considered. The density profiles in the region near mach stems of the computational results are given in Fig.17. Like in the previous results, PORWENO9-S and PORWENO17-S obtain more small scale structures than WENO5-M. And the differences between PORWENO9-S and PORWENO17-S are also very small. Note that the carbuncle phenomenon near the mach stem almost never appears in these results which however could be seen clearly in those of RORWENO schemes with fine grid as shown in Fig.20 of [8].

(5) The Rayleigh-Taylor instability problem is taken into consideration[47]. This instability is driven by the gravity and happens on the interface between fluids with different densities. The source term  $[0, 0, \rho, \rho v]^T$  in the right hand side of the governing equations represent the effect of gravity. The computational domain is  $[0, 0.25] \times [0, 1]$ , and the initial state is

$$(\rho, u, v, p) = \begin{cases} (1, 0, -0.025c \cos(8\pi x), y + 1.5), & y \geq 0.5, \\ (2, 0, -0.025c \cos(8\pi x), 2y + 1), & y < 0.5. \end{cases} \quad (72)$$

where  $c = \sqrt{\gamma p / \rho}$  is the sound speed. Note that  $\gamma$  is set as  $5/3$  in this test case. The reflecting boundary conditions are imposed for the left and right boundaries.  $(\rho, u, v, p)$  is set as  $(1, 0, 0, 2.5)$  and  $(2, 0, 0, 1)$  at the top and bottom boundary respectively. The end time of the simulation is  $t = 1.95$ . Even though the effect of gravity should be taken into consideration for criterion Eq.(56), the order reduction procedure is not modified here and the computations have been safely accomplished. WENO5-M, PORWENO9-S, PORWENO13-S and PORWENO17-S schemes are tested with grids  $N_x \times N_y = 120 \times 480, 240 \times 960$ . The density contours of numerical results are shown in Fig.18. The three PORWENO-S schemes also obtain close results which have slightly more small structures compared with the WENO5-M scheme.

## 8 Conclusions

In the present study, a class of very high order WENO schemes which was the extension of WENO7-S were proposed. By using a class of efficient smoothness indicators, these new schemes have some advantages over the classical very high order WENO schemes. Firstly, they are more time efficient and less error prone for programming. The second is that they have the same approximate dispersion relation (ADR) as their underlying linear schemes, which will be helpful for problems with profiles close to sinusoid. The third is that they have both good behavior near critical points and good stability near discontinuities.

According to the numerical results in 1D scalar tests, the proposed very high order WENO-S schemes obtain much better results than the classical ones. Furthermore, the proposed schemes require only about 50% to 75%

Figure 16: Numerical results at  $t = 0.8$  of three different schemes for a 2D Riemann problem, density contours. From left to right: WENO5-M, PORWENO9-S and PORWENO17-S.

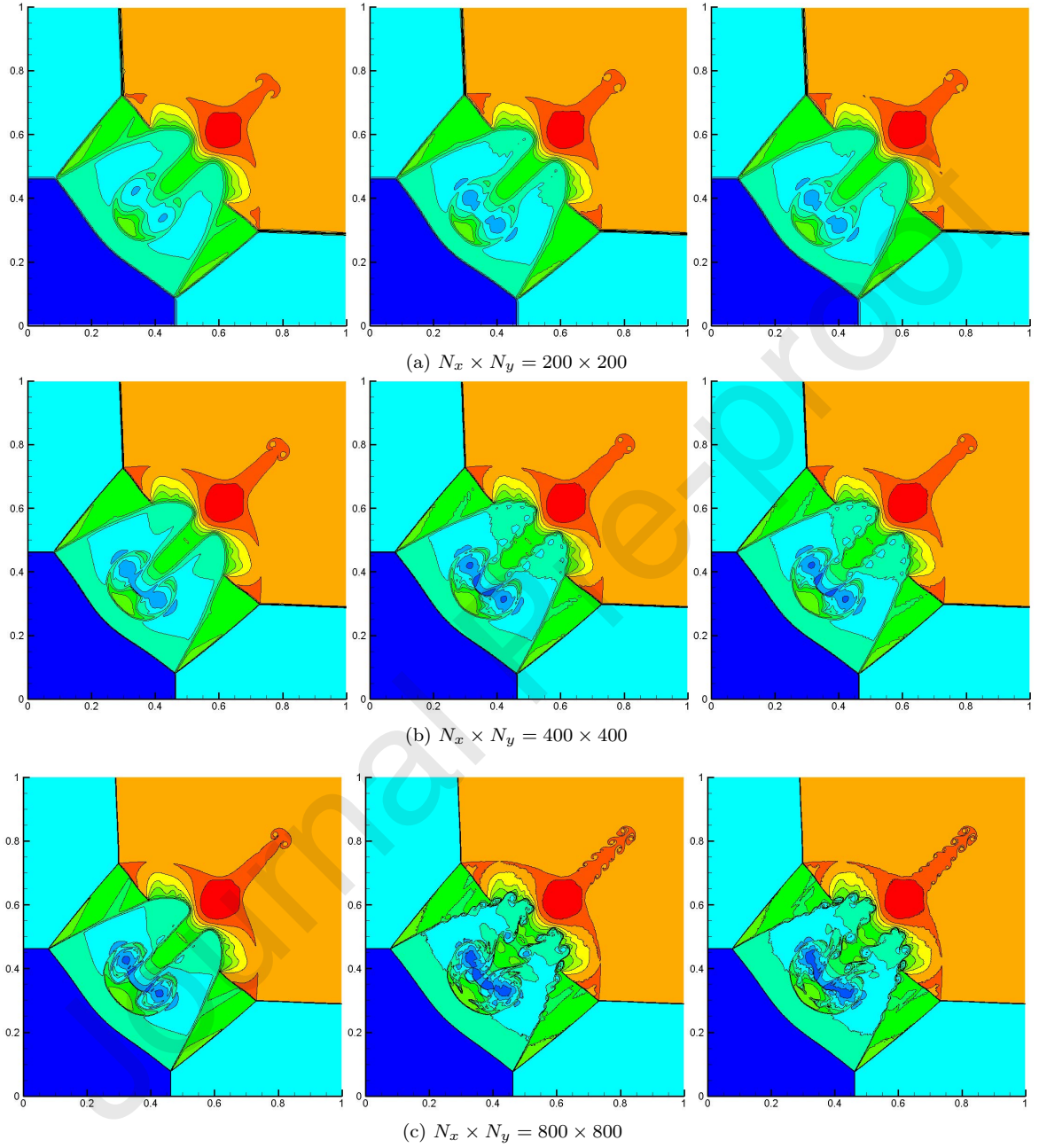




Figure 17: Numerical results in the region near mach stems at  $t = 0.2$  of three different schemes for double Mach reflection problem, density contours. From left to right: WENO5-M, PORWENO9-S and PORWENO17-S.

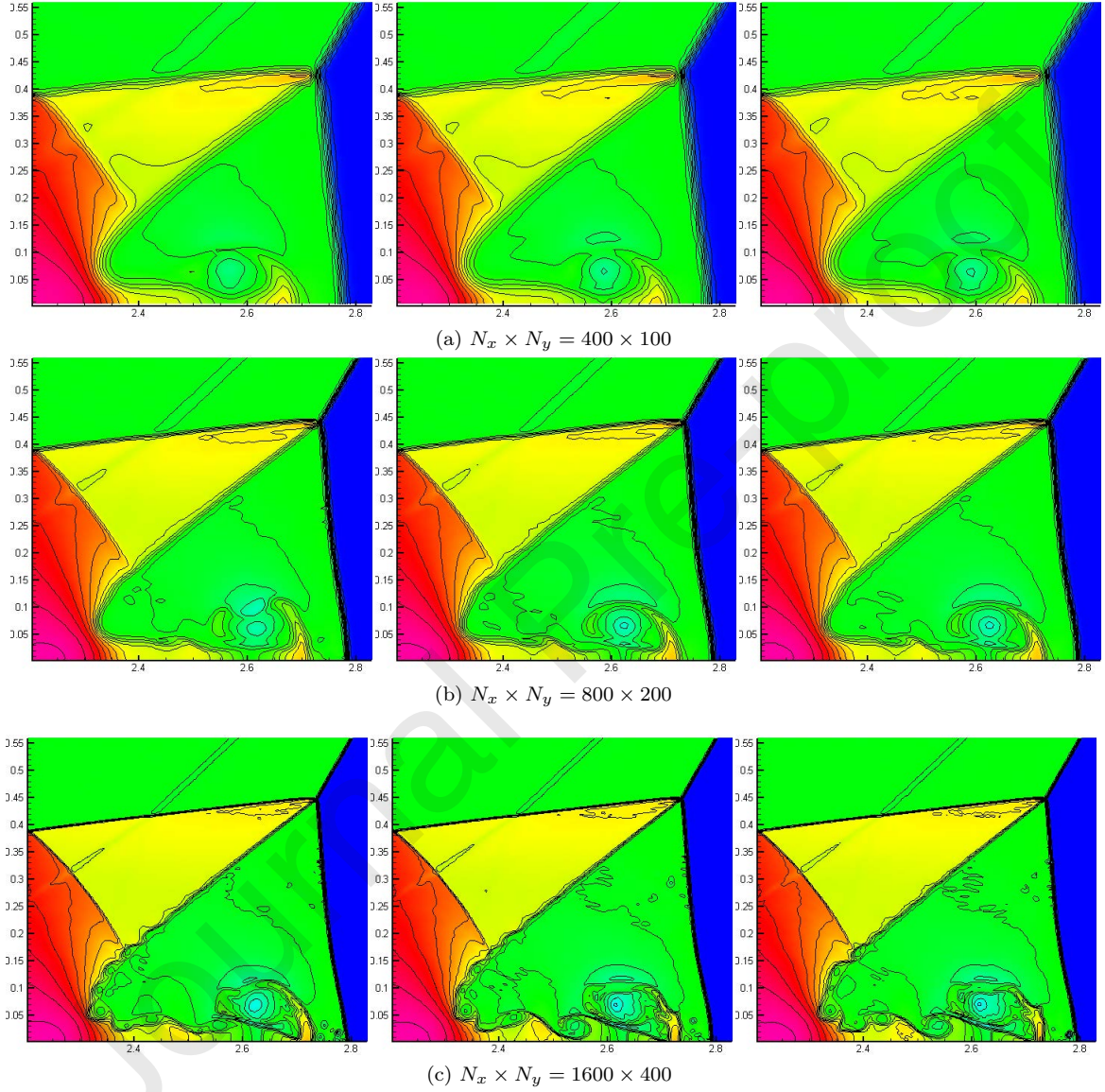
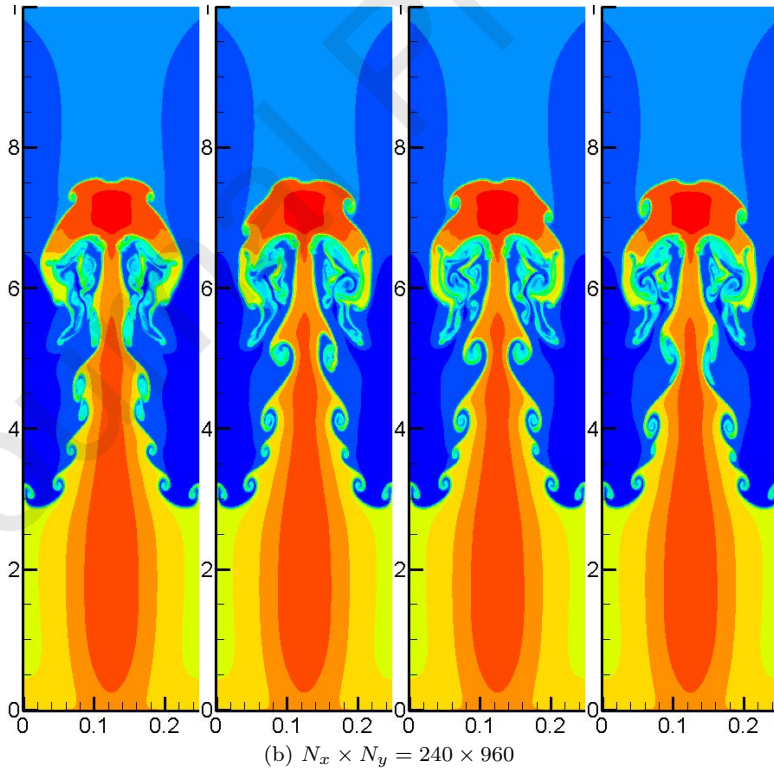
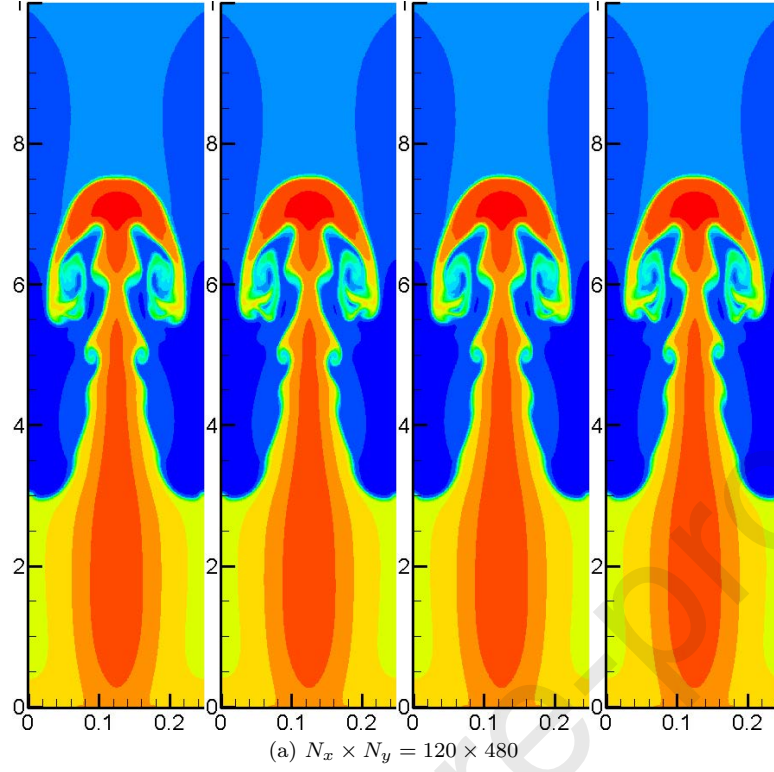




Figure 18: Numerical results at  $t = 1.95$  of three different schemes for Rayleigh-Taylor instability problem, density contours. From left to right: WENO5-M, PORWENO9-S, PORWENO13-S and PORWENO17-S.



CPU time of those of the classical ones for 1D advection problem. As for the very high order FWENO schemes, they have poor stability and are more likely to be blow up in the numerical simulations.

For Euler equations, a predetermined order reduction method has been employed to suppress the non-physical oscillations and to prevent the emergence of negative pressure. The proposed schemes with this technique are called as PORWENO-S schemes. The criterion to prevent non-physical oscillations is that the smoothness indicator of pressure on the stencil needed for the flux is less than 4 times of that on the stencil without two ending points. To prevent the emergence of the negative pressure, another inequality is proposed according to the governing equation of the pressure. The minimum order of this procedure is constrained to 5 in the present work, since the fifth order WENO scheme is robust enough for most problems. As the accuracy order is reduced to 5, WENO5-M is employed because WENO(2r-1)-S schemes are only available for  $r \geq 4$ . The criterion with both two considerations works well in the numerical tests. The numerical results show that the proposed PORWENO-S schemes can obtain better results than WENO5-M schemes, and the differences among these PORWENO-S schemes are very small.

Let us reexamine the 1D scalar cases, the WENO(2r-1)-S schemes obtain almost the same results for  $r \geq 7$ . That means WENO(2r-1)-S schemes with  $r > 7$  has little advantage over those  $r = 7$  except the convergence order. Thus, WENO(2r-1)-S and PORWENO(2r-1)-S schemes with  $r = 8, 9$  or even larger  $r$  are not suggested in the practical use.

The smoothness indicators employed in this work have been shown more effective than the classical ones. Then, these smoothness indicators could also be adopted in other shock capturing methods like TENO[29] and AOWENO[30] schemes. Because of the differences between two kinds of smoothness indicators, these works need further investigations.

## Acknowledgements

This work is supported by National Numerical Windtunnel project, National Natural Science Foundation of China under research grant 11732016 and Sichuan Science and Technology Program under research grant 2018JZ0076.

## Appendix

### 1. A method to obtain the expression of numerical flux

In a conservative difference scheme, the numerical flux  $\hat{f}_{i+1/2}$  is not obtained by interpolating  $f(x)$  at  $x_{i+1/2}$ . The procedure from  $(m+n+1)$  node values  $f_{i-m}, \dots, f_{i+n}$  to the numerical flux  $\hat{f}_{i+1/2}$  is often called as reconstruction. First, a function  $s(x)$  could be given implicitly as

$$f(x) = \frac{1}{h} \int_{x-h/2}^{x+h/2} s(z) dz. \quad (73)$$

Then we have

$$f'(x) = \frac{1}{h} (s(x+h/2) - s(x-h/2)) \quad (74)$$

Therefore the numerical flux  $\hat{f}_{i+1/2}$  can be viewed as an approximation of  $s(x)$ . Now we will consider how to obtain  $\hat{f}_{i+1/2}$ . Let us use a polynomial to approximate  $s(x)$

$$\tilde{s}(x) = \sum_{k=0}^{m+n} a_k x^k. \quad (75)$$

Thus, we could obtain an approximation of  $f(x)$ ,

$$\tilde{f}(x) = \frac{1}{h} \int_{x-h/2}^{x+h/2} \tilde{s}(z) dz = \sum_{k=0}^{m+n} b_k x^k. \quad (76)$$

The relation between  $\{a_k\}$  and  $\{b_k\}$  could be represented as

$$C \cdot [a_0, \dots, a_{m+n}]^T = [b_0, \dots, b_{m+n}]^T, \quad (77)$$

where the matrix  $C$  can be obtained by some manipulations.

Then, according to the  $(m+n+1)$  known node values,  $(m+n+1)$  equations could be obtained using Eq.(76). Thus the coefficients  $\{b_k\}$  could be obtained by solving the linear system of these equations. Then  $\{a_k\}$  could

Table 15: The matrix  $C_{k,r}$  and  $\Lambda_{k,r}$  in Eqs. (78) of classical smoothness indicators  $\beta_k^{r(JS)}$  for  $r = 3, 4$ .

$k$	$r = 3$			
0	$\Lambda_{k,r}$	$diag(2\sqrt{3}/3, \sqrt{13}/4)$		
	$C_{k,r}$	$\begin{bmatrix} 1 & -19/8 & 11/8 \\ 0 & 1 & -1 \end{bmatrix}$		
1	$\Lambda_{k,r}$	$diag(2\sqrt{3}/3, \sqrt{13}/4)$		
	$C_{k,r}$	$\begin{bmatrix} 1 & -13/8 & 5/8 \\ 0 & 1 & -1 \end{bmatrix}$		
2	$\Lambda_{k,r}$	$diag(\sqrt{30}/3, \sqrt{130}/20)$		
	$C_{k,r}$	$\begin{bmatrix} 1 & -31/20 & 11/20 \\ 0 & 1 & -1 \end{bmatrix}$		
$r = 4$				
0	$\Lambda_{k,r}$	$diag(\sqrt{8205}/60, \sqrt{1744383}/1641, \sqrt{32377917}/6378)$		
	$C_{k,r}$	$\begin{bmatrix} 1 & -1941/547 & 2321/547 & -927/547 \\ 0 & 1 & -5293/2126 & 3167/2126 \\ 0 & 0 & 1 & -1 \end{bmatrix}$		
1	$\Lambda_{k,r}$	$diag(\sqrt{445}/20, \sqrt{94607}/267, \sqrt{32377917}/6378)$		
	$C_{k,r}$	$\begin{bmatrix} 1 & -821/267 & 3 & -821/267 \\ 0 & 1 & -3471/2126 & 1345/2126 \\ 0 & 0 & 1 & -1 \end{bmatrix}$		
2	$\Lambda_{k,r}$	$diag(\sqrt{8205}/60, \sqrt{6014265}/1641, \sqrt{111632235}/21990)$		
	$C_{k,r}$	$\begin{bmatrix} 1 & -1261/547 & 961/547 & -247/547 \\ 0 & 1 & -10497/7330 & 3167/7330 \\ 0 & 0 & 1 & -1 \end{bmatrix}$		
3	$\Lambda_{k,r}$	$diag(7\sqrt{645}/60, \sqrt{1747821}/903, \sqrt{412688991}/81294)$		
	$C_{k,r}$	$\begin{bmatrix} 1 & -4701/2107 & 503/301 & -927/2107 \\ 0 & 1 & -40411/27098 & 13313/27098 \\ 0 & 0 & 1 & -1 \end{bmatrix}$		

also be obtained by solving Eq.(77). The numerical flux will be  $\sum_{k=0}^{m+n} a_k(x_i + h/2)^k$ , and it should be in a form  $\hat{f}_{i+1/2} = \sum_{k=-m}^n c_k f_{i+k}$ . Thus, the coefficients  $c_k$ ,  $k = -m, \dots, n$  are obtained.

To simplify this procedure,  $x_i$  could be set as 0, and  $h$  could be set as 1. This will not alter the results. If many node points have been used to reconstruct the numerical flux, this procedure is tedious and error prone, and a computer program using symbolic computation is suggested for this work.

## 2. The classical smoothness indicators in non-negative definite quadratic form

The classical smoothness indicators can also be written in non-negative definite quadratic form as Eq.(10)[32]. The upper triangular matrix  $B_{k,r}$  of smoothness indicator  $\beta_k^{r(JS)}$  will be given here. By using symbolic computation, the elements in the last line of  $B_{k,r}$  are found to be zero for  $r = 3, \dots, 9$ . To get a better display, every line of  $B_{k,r}$  is normalized by its diagonal element. Let

$$B_{k,r} = \begin{bmatrix} \Lambda_{k,r} C_{k,r} \\ 0 \dots 0 \end{bmatrix}, \quad r = 3, 4, \dots, 9, \quad (78)$$

where  $C_{k,r}$  is a  $r \times (r-1)$  matrix and  $\Lambda_{k,r}$  is the diagonal matrix which is composed of the first  $(r-1)$  diagonal elements of  $B_{k,r}$ . Then  $C_{k,r}$  and  $\Lambda_{k,r}$  for  $r = 3, 4, 5$  are shown in Tables 15,16,17. Because the case of  $r = 2$  just leads to Eq.(8), it does not be given here. As for higher value  $r$ , the coefficients of  $B_{k,r}$  are very complex and do not be given here.

## References

- [1] A. Harten, High resolution schemes for conservation laws, J. Comput. Phys., 49 (1983) 357-393.

Table 16: The diagonal elements of  $\Lambda_{k,r}$  in Eq. (78) of classical smoothness indicators  $\beta_k^{r(JS)}$  for  $r = 5$ .

$k$	Diagonal elements
0	$(\sqrt{793030}/420, \sqrt{193716587562}/543792, 2\sqrt{248759756350023}/42747945, \sqrt{96904093308502161}/349153284)$
1	$(\sqrt{60445}/210, \sqrt{677061715}/27632, 2\sqrt{11406983268815}/5880675, \sqrt{96904093308502161}/349153284)$
2	$(\sqrt{60445}/210, \sqrt{14765140203}/82896, \sqrt{12846941339118}/2514585, \sqrt{1446303987150483714}/2605575108)$
3	$(\sqrt{793030}/420, 7\sqrt{30758438922}/543792, \sqrt{2862368513038002}/47512815, \sqrt{7022472797218781694}/12651268668)$
4	$(\sqrt{3777130}/420, \sqrt{6405506236662}/863344, 2\sqrt{132391829280434178}/890329635, \sqrt{7428632088185797566}/26765962104)$

Table 17: The matrix  $C_{k,r}$  in Eqs.(78) of classical smoothness indicators  $\beta_k^{r(JS)}$  for  $r = 5$ .

$k$	$C_{k,r}$				
0	1	$-208501/45316$	$364863/45316$	$-288007/45316$	$86329/45316$
	0	1	$-55338513/14249315$	$71911201/14249315$	$-1813059/838195$
	0	0	1	$-583582777/232768856$	$350813921/232768856$
	0	0	0	1	-1
1	1	$-60871/13816$	$99213/13816$	$-70237/13816$	$18079/13816$
	0	1	$-18329233/5880675$	$67923/22025$	$-5686883/5880675$
	0	0	1	$-379530087/232768856$	$146761231/232768856$
	0	0	0	1	-1
2	1	$-51001/13816$	$67923/13816$	$-38947/13816$	$8209/13816$
	0	1	$-1870849/838195$	$23242001/14249315$	$-5686883/14249315$
	0	0	1	$-71725821/51089708$	$20636113/51089708$
	0	0	0	1	-1
3	1	$-140251/45316$	$165153/45316$	$-88297/45316$	$18079/45316$
	0	1	$-217591953/110863235$	$19650103/15837605$	$-30822003/110863235$
	0	0	1	$-5962732027/4217089556$	$1745642471/4217089556$
	0	0	0	1	-1
4	1	$-649501/215836$	$758823/215836$	$-411487/215836$	$86329/215836$
	0	1	$-1835635153/890329635$	$411792427/296776545$	$-290071763/890329635$
	0	0	1	$-26228937057/17843974736$	$8384962321/17843974736$
	0	0	0	1	-1

- [2] A. Harten, B. Engquist, S. Osher, S.R. Chakravarthy, Uniformly high order accurate essentially nonoscillatory schemes III, *J. Comput. Phys.* 71 (1987) 231–303.
- [3] A. Suresh, H. T. Huynh, Accurate monotonicity preserving scheme with Runge-kutta time-stepping, *J. Comput. Phys.* 136 (1997) 83–99.
- [4] C.W. Shu, High order weighted essentially non-oscillatory schemes for convection dominated problems, *SIAM Rev.* 51 (2009) 82–126.
- [5] X.D. Liu, S. Osher, T. Chan, Weighted essentially non-oscillatory schemes, *J. Comput. Phys.* 115 (1994) 200–212.
- [6] G. Jiang, C.W. Shu, Efficient implementation of weighted ENO schemes, *J. Comput. Phys.* 126 (1996) 202–228.
- [7] D.S. Balsara, C.W. Shu, Monotonicity preserving WENO schemes with increasingly high order of accuracy, *J. Comput. Phys.* 160 (2000) 405–452.
- [8] G.A. Gerolymos, D. Sénéchal, I. Vallet, Very-high order WENO schemes, *J. Comput. Phys.* 228 (2009) 8481–8524.
- [9] A.K. Henrick, T.D. Aslam, J.M. Powers, Mapped weighted-essentially-non-oscillatory schemes: achieving optimal order near critical points, *J. Comput. Phys.* 207 (2005) 542–567.
- [10] R. Borges, M. Carmona, B. Costa, W.S. Don, An improved weighted essentially non-oscillatory scheme for hyperbolic conservation laws, *J. Comput. Phys.* 227 (2008) 3191–3211.
- [11] M. Castro, B. Costa, W.S. Don, High order weighted essentially non-oscillatory WENO-Z schemes for hyperbolic conservation laws, *J. Comput. Phys.* 230 (2011) 1766–1792.
- [12] F. Acker, R. B.de R. Borges, B. Costa, An improved WENO-Z scheme, *J. Comput. Phys.* 313 (2016) 726–753.
- [13] Y. Ha, C.H. Kim, Y.J. Lee, J. Yoon, An improved weighted essentially non-oscillatory scheme with a new smoothness indicator, *J. Comput. Phys.* 232 (2013) 68–86.
- [14] C.H. Wu, L. Wu, S.H. Zhang, A smoothness indicator constant for sine functions, *J. Comput. Phys.* 419 (2020) 109661.
- [15] S. Zhao, N. Lardjane, I. Fedioun, Comparison of improved finite-difference WENO schemes for the implicit large eddy simulation of turbulent non-reacting and reacting high-speed shear flows, *Comput. Fluids*, 95 (2014) 74–87.
- [16] M.P. Martin, E.M. Taylor, M. Wu, V.G. Weirs, A bandwidth-optimized WENO scheme for the effective direct numerical simulation of compressive turbulence, *J. Comput. Phys.* 220 (2006) 270–289.
- [17] X.Y. Hu, Q. Wang, N.A. Adams, An adaptive central-upwind weighted essentially non-oscillatory scheme, *J. Comput. Phys.* 229 (2010) 8952–8965.
- [18] J. Zhu, J. Qiu, A new fifth order finite difference WENO scheme for solving hyperbolic conservation laws, *J. Comput. Phys.* 318 (2016) 110–121.
- [19] J.X. Qiu, C.W. Shu, Hermite WENO schemes and their application as limiters for Runge-Kutta discontinuous Galerkin method: one-dimensional case, *J. Comput. Phys.* 193 (2003) 115–135.
- [20] B. Costa, W.S. Don, High order hybrid central-WENO finite difference scheme for conservation laws, *J. Comput. Appl. Math.*, 204 (2007) 209–218.
- [21] S. Pirozzoli, Conservative hybrid compact-WENO schemes for shock-turbulence interaction, *J. Comput. Phys.*, 178 (2001): 81–117.
- [22] Y. X. Ren, M. Liu and H. X. Zhang, A characteristic-wise hybrid compact-WENO scheme for solving hyperbolic conservation laws, *J. Comput. Phys.*, 192 (2003) 365–386.
- [23] C.H. Wu, S.J. Yang, N. Zhao, A fifth order low-dissipative conservative upwind compact scheme using centered stencil, *Adv. Appl. Math. Mech.*, 6 (6) (2014) 830–848.
- [24] C.H. Wu, N. Zhao, L.L. Tian, An improved hybrid compact-WENO scheme, *Acta Aerodyn. Sin.*, 31(4) (2014) 477–481.

- [25] X.G. Deng, H.X. Zhang, Developing high order weighted compact nonlinear schemes, *J. Comput. Phys.*, 165 (2000) 22-44.
- [26] S.H. Zhang, S.F. Jiang, C.W. Shu, Development of nonlinear weighted compact schemes with increasingly higher order accuracy, *J. Comput. Phys.*, 227 (2008) 7294-7321.
- [27] Z.J. Wang, R.F. Chen, Optimized weighted essentially non-oscillatory schemes for linear waves with discontinuity, *J. Comput. Phys.*, 174 (2001) 381-404.
- [28] Y.T. Zhang, J. Shi, C.W. Shu, Y. Zhou, Numerical viscosity and resolution of high order weighted essentially nonoscillatory schemes for compressible flows with high Reynolds numbers, *Phys. Rev. E.*, 68 (2003) 046709.
- [29] L. Fu, X.Y. Hu, N.A. Adams, A family of high order targeted ENO schemes for compressible-fluid simulations, *J. Comput. Phys.* 305(2016) 333-359.
- [30] D.S. Balsara, S. Garain, C.W. Shu, An efficient class of WENO schemes with adaptive order, *J. Comput. Phys.* 326 (2016) 780-804.
- [31] D.S. Balsara, T. Rumpf, M. Dumbser, C.-D. Munz, Efficient high-accuracy ADER-WENO schemes for hydrodynamics and divergence-free magnetohydrodynamics, *J. Comput. Phys.* 228 (2009) 2480.
- [32] A. Baeza, R. Burger, P. Mulet, D. Zorío, On the efficient computation of smoothness indicators for a class of WENO reconstructions, *J. Sci. Comput.*, 80(2019) 1240-1263.
- [33] S. Gottlieb, C.W. Shu, E. Tadmor, Strong stability preserving high order time discretization methods, *SIAM Rev.* 43,1 (2001) 89-112.
- [34] W.S. Don, R. Borges, Accuracy of the weighted essentially non-oscillatory conservative finite difference schemes, *J. Comput. Phys.*, 250 (2013) 347-372.
- [35] S. Pirozzoli, On the spectral properties of shock-capturing schemes. *J. Comput. Phys.*, 219 (2006) 489 - 497.
- [36] S. Gottlieb, L. A. J. Gottlieb, Strong stability preserving properties of Runge-Kutta time discretization methods for linear constant coefficient operators, *J.Sci. Comput.* 18 (1) (2003) 83-109.
- [37] S. Gottlieb, On high order strong stability preserving Runge-Kutta and multistep time discretizations, *J. Sci. Comput.* 25 (1) (2005) 105-128.
- [38] G. M. Arshed, K. A. Hoffmann, Minimizing errors from linear and nonlinear weights of WENO scheme for broadband applications with shock waves, *J. Comput. Phys.*, 246 (2013) 58-77.
- [39] G.Y. Zhao, M.B. Suna, A. Memmolo, S. Pirozzoli, A general framework for the evaluation of shock-capturing schemes, *J. Comput. Phys.*, 376 (2019) 924-936.
- [40] J. Casper, M.H. Carpenter, Computational considerations for the simulation of shock-induced sound, *SIAM J. Sci. Comput.* 19 (1998) 813-828.
- [41] D.P. Lockard, K.S. Brentner, H.L. Atkins, High accuracy algorithms for computational aeroacoustics, *AIAA J.*, 33, 2(1995) 246-251.
- [42] J.J. Quirk, A contribution to the great Riemann solver debate, *Int. J. Numer. Meth. Fl.* 18(6) (1994) 555-574.
- [43] H.Z. Tang, T.G. Liu, A note on the conservative schemes for the Euler equations, *J. Comput. Phys.*, 218 (2006) 451-459.
- [44] P. Woodward, P. Collela, The numerical simulation of two dimensional fluid flow with strong shocks, *J. Comput. Phys.*, 54(1984) 115-173.
- [45] P.D. Lax, X.D. Liu, Solution of two-dimensional Riemann problems of gas dynamics by positive schemes, *SIAM J. Sci. Comput.* 19(2) (1998) 319-340.
- [46] C.W. Schulz-Rinne, J.P. Collins, H.M. Glaz, Numerical solution of the Riemann problem for two dimensional gas dynamics, *SIAM J. Sci. Comput.* 14(6) (1993) 1394-1414.
- [47] J. Shi, Y.T. Zhang, C.W. Shu, Resolution of high order WENO schemes for complicated flow structures, *J. Comput. Phys.* 186 (2) (2003) 690-696.

**Declaration of interests**

☒ The authors declare that they have no known competing financial interests or personal relationships that could have appeared to influence the work reported in this paper.

☐ The authors declare the following financial interests/personal relationships which may be considered as potential competing interests:

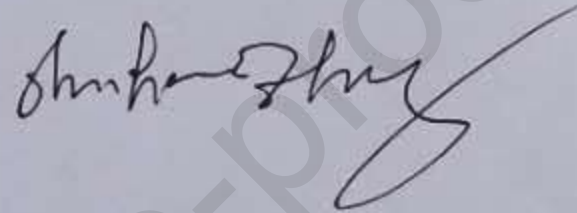
--

### Conflict of interest statement

We declare that we have no financial and personal relationships with other people or organizations that can inappropriately influence our work, there is no professional or other personal interest of any nature or kind in any product, service and/or company that could be construed as influencing the position presented in, or the review of, the manuscript entitled "Very high order WENO schemes using efficient smoothness indicators" .

Signed by all authors as follows:

Congkai Wu , Ling Wu

Hu Li , 



## Credit author statement

January 26, 2021

Conghai Wu: Conceptualization, Methodology, Formal analysis, Software, Writing- Original draft preparation.

Ling Wu: Visualization, Validation.

Hu Li: Data Curation.

Shuhai Zhang: Writing- Reviewing and Editing.